Article

Cell Reports

Hierarchy in Hfq Chaperon Occupancy of Small RNA Targets Plays a Major Role in Their Regulation

Graphical Abstract

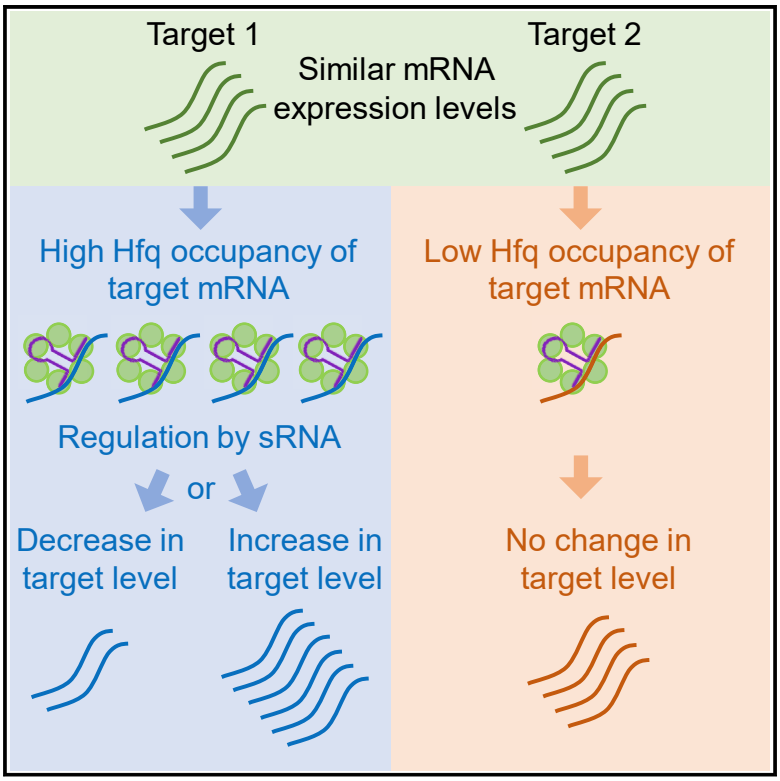

Authors

Raya Faigenbaum-Romm, Avichai Reich, Yair E. Gatt, Meshi Barsheshet, Liron Argaman, Hanah Margalit

Correspondence

hanahm@ekmd.huji.ac.il

In Brief

Faigenbaum-Romm et al. analyze data of sRNA-target pairs and transcriptome measurements, revealing that only a subset of targets shows expression changes under overexpression of the sRNA. Analyzing various target features, they find that competition among targets over binding the chaperon Hfq plays a major role in the regulatory outcome.

Highlights

- Basic concepts of regulation by small RNAs are revealed from large-scale data
- Small changes in the small RNA sequence shift the target repertoire accordingly
- A regulatory sRNA affects the expression levels of only a subset of its targets
- Competition among targets over Hfq binding plays a major role in their regulation

Faigenbaum-Romm et al., 2020, Cell Reports *30*, 3127–3138
March 3, 2020
https://doi.org/10.1016/j.celrep.2020.02.016

CellPress

Cell Reports
Article

Hierarchy in Hfq Chaperon Occupancy of Small RNA Targets Plays a Major Role in Their Regulation

Raya Faigenbaum-Romm,[1] Avichai Reich,[1,2] Yair E. Gatt,[1,2] Meshi Barsheshet,[1] Liron Argaman,[1] and Hanah Margalit[1,3,*]
[1]Department of Microbiology and Molecular Genetics, Institute for Medical Research Israel-Canada, Faculty of Medicine, The Hebrew University of Jerusalem, Jerusalem 9112102, Israel
[2]These authors contributed equally
[3]Lead Contact
*Correspondence: hanahm@ekmd.huji.ac.il
https://doi.org/10.1016/j.celrep.2020.02.016

SUMMARY

Bacterial small RNAs (sRNAs) are posttranscriptional regulators of gene expression that base pair with complementary sequences on target mRNAs, often in association with the chaperone Hfq. Here, using experimentally identified sRNA-target pairs, along with gene expression measurements, we assess basic principles of regulation by sRNAs. We show that the sRNA sequence dictates the target repertoire, as point mutations in the sRNA shift the target set correspondingly. We distinguish two subsets of targets: targets showing changes in expression levels under overexpression of their sRNA regulator and unaffected targets that interact more sporadically with the sRNA. These differences among targets are associated with their Hfq occupancy, rather than with the sRNA-target base-pairing potential. Our results suggest that competition among targets over Hfq binding plays a major role in the regulatory outcome, possibly awarding targets with higher Hfq binding efficiency an advantage in the competition over binding to the sRNA.

INTRODUCTION

Small RNAs (sRNAs) are major posttranscriptional regulators of gene expression in bacteria. They play important roles in bacterial adaptation to various stress conditions (Wagner and Romby, 2015). These 50- to 400-nucleotide-long RNAs serve as negative or positive regulators of their targets by base pairing with their mRNAs, usually in association with the chaperone protein Hfq (Vogel and Luisi, 2011). Hfq binds both the sRNA and the mRNA and stimulates their pairing (Groszewska et al., 2016; Updegrove et al., 2016). A major challenge has been to identify sRNA targets and study the principles of sRNA-target regulation. Conventionally, two main features were used to define a gene as a putative target of a sRNA: (1) sequence complementarity between the gene transcript and the sRNA and (2) an observed change in the expression level of the gene following an expression change of the sRNA. These two features usually have been combined in target determination (e.g., De Lay and Gottesman, 2009; Kery et al., 2014; Papenfort et al., 2009; Wright et al., 2014). In addition, targets of sRNAs could be postulated from results of Hfq immunoprecipitation experiments (Holmqvist et al., 2016; Tree et al., 2014), in which possible pairing between extracted RNAs was supported by sequence complementarity considerations.

Recently, we developed RIL-seq (RNA Interaction by Ligation and sequencing), an experimental-computational high-throughput methodology for *in vivo* capturing of Hfq-mediated sRNA-target interactions that is independent of gene expression and sequence considerations (Melamed et al., 2016, 2018). The experimental part of RIL-seq involves ligation of Hfq-bound RNAs, RNA isolation, and sequencing. The computational part involves mapping the sequenced fragments to the genome and identifying statistically significant chimeric fragments, which represent putative RNA-RNA interacting pairs. Application of RIL-seq to *Escherichia coli* grown under three growth conditions resulted in the identification of ~2,800 unique interacting pairs, two-thirds of which involved known sRNAs. This objective dataset of sRNA-target pairs, captured *in vivo* under specific conditions, enables the assessment of basic concepts of sRNA-target binding and regulation while considering the influence of all sRNA-target interactions.

Application of the RIL-seq methodology provides data of Hfq-bound sRNA-target duplexes, but it does not reveal the regulatory outcome of the various interactions, i.e., whether the sRNA increases or decreases the target expression level. It is possible to obtain this information by measuring changes in gene expression levels upon change in the expression level of a studied sRNA. It is widely accepted that sRNAs may affect both the protein level and the mRNA level of their targets. Therefore, changes in mRNA levels following overexpression or deletion of a sRNA often have been used as a proxy for the effect a sRNA has on its targets (Hör et al., 2018). Here we conducted such experiments and, surprisingly, discovered that not all targets revealed by RIL-seq in duplexes with a sRNA show a change in their expression level following overexpression of the respective sRNA. We describe these results and analyze possible distinguishing features between the targets that demonstrated an expression change and the ones that did not in an attempt to reveal the underlying principles of the regulatory outcome. Our results suggest that differences in Hfq occupancy of target transcripts under a studied condition play a major role in determining the different regulatory impacts a sRNA has on its targets.

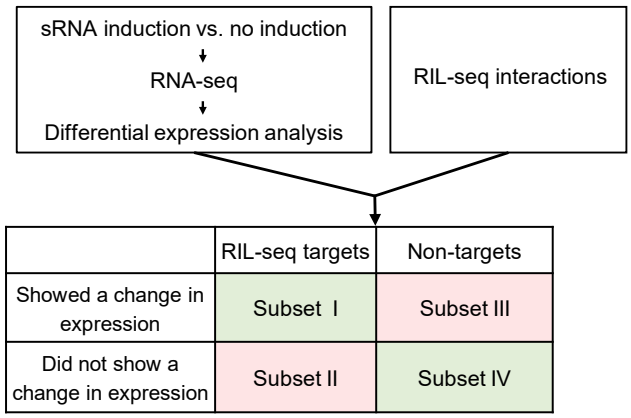

Figure 1. Schematic Description of the Study and Generated Data

RNA-seq experiments were performed on samples with and without sRNA overexpression. Differential expression analysis was conducted, and the results were intersected with RIL-seq interactions of the studied sRNA under the same growth condition as in the RNA-seq experiment (Melamed et al., 2016). Four subsets of genes could be discerned: two with an expected regulatory outcome (I and IV, marked in green) and two with an unexpected outcome (II and III, marked in pink). See also Figure S4 and Tables S1, S2, S3, and S4.

RESULTS

The sRNA Affects the Expression Levels of Only a Subset of Targets

To study the regulatory outcome of Hfq-mediated sRNA-target interaction, we measured the change in gene expression following overexpression of each of five well-established sRNAs: GcvB, MicA, ArcZ, RyhB, and CyaR. We compared the transcriptomes of two types of strains: (1) a strain in which the sRNA is induced for a short time, either from an inducible plasmid (in the studies of GcvB, MicA, ArcZ, and CyaR) or from the endogenous chromosomal locus (in the study of RyhB), and (2) a control strain in which the sRNA is not induced (STAR Methods). The sRNAs were studied in the phase and growth condition in which their native expression level is known to be high to ensure that their targets are expressed as well. Expression of GcvB was induced in the exponential phase (Argaman et al., 2001; Sharma et al., 2007), that of RyhB was induced in the exponential phase under iron limitation (Jacques et al., 2006), and that of ArcZ, MicA, and CyaR was induced in the stationary phase (Argaman et al., 2001; De Lay and Gottesman, 2009). Comparison of gene expression levels between the two strain types by DESeq2 analysis (Love et al., 2014) resulted in the determination of four gene subsets (Figures 1 and 2A; Table S1): (I) RIL-seq targets that showed a statistically significant change in expression level following the sRNA overexpression, (II) RIL-seq targets that did not exhibit a statistically significant change in their expression level, (III) non-target genes that showed a statistically significant change in their expression level, and (IV) non-target genes that did not show a statistically significant change in their expression level. The results for subset I and subset IV were as expected; the expression levels of targets of the sRNA changed in response to the sRNA, whereas non-targets did not show an expression change. The results for subsets II and III were surprising, raising two main questions: (1) What underlies the change in expression levels of the non-targets in subset III? (2) What differences between the targets in subset I and those in subset II may underlie their different responses to the sRNA? We briefly address the first question and in the rest of the paper elaborate on the second question, attempting to reveal the features that determine the regulatory outcome of sRNA-target interaction.

We comprehensively analyzed the non-target genes in subset III and could ascribe possible explanations to the change in expression levels for several genes in this group (Table S2). First, some of these genes were detected as targets of the sRNA but under another growth condition (e.g., GcvB targets discovered by RIL-seq in the stationary phase). Second, some genes appear in operons in which the first gene is a target of the sRNA. For example, several of GcvB's targets are first in their respective operons, *oppA*, *dppA*, *gltI*, *livK*, and *panB*, and 15 of the non-target genes exhibiting an expression change are encoded in these operons (Santos-Zavaleta et al., 2019). Third, some genes were affected by the sRNA indirectly, because one of their regulators (transcription factor or sigma factor) is a target. For example, FliA, the sigma factor of flagella genes, is a target of ArcZ and regulates several genes that exhibited a decrease in expression under ArcZ overexpression, such as *flgN*. It is also possible that some genes in subset III are true targets of the studied sRNA that were missed by RIL-seq and might be revealed in deeper RIL-seq screens or when the sRNA in the RIL-seq experiment is expressed in high levels, as in the transcriptome experiment. Finally, under overexpression of a given sRNA, some other sRNAs showed a decreased expression level, presumably because their binding to Hfq was reduced due to the competition with the overexpressed sRNA. For example, 11 sRNAs were downregulated following overexpression of GcvB.

As shown in Figure 2B, for most sRNAs, the fraction of RIL-seq targets among the genes showing an expression change was statistically significantly higher than the general fraction of the targets in the genome ($p < 10^{-25}$ to $p < 0.02$ by hypergeometric test for the various sRNAs) (Figure 2B; Tables S1 and S3). Yet some RIL-seq targets did not exhibit a change in expression level upon overexpression of the sRNA under the studied conditions (subset II, Figures 1 and 2A; Tables S1 and S4). The DESeq2 algorithm enables a finer dissection of these targets, pointing out the targets that were statistically significantly unchanged in their expression levels (Love et al., 2014). Thus, we define two target subsets for further analysis: targets that showed a statistically significant change in expression (hereinafter, affected targets) and targets that were statistically significantly unchanged in their expression levels (hereinafter, unaffected targets). Targets that could not be assigned unambiguously to either of the two groups were excluded from further analysis (Table S4).

The targets identified as unaffected at the RNA level may be affected at the protein level, as was demonstrated for RyhB by Wang et al. (2015). In that study, Wang et al. (2015) assessed changes in RNA expression levels and in ribosome profiling measures following overexpression of RyhB, attempting to identify targets that show a change in their transcription and/or translation level. We identified in the data of Wang et al. (2015) seven RIL-seq RyhB targets that showed a change in their RNA levels

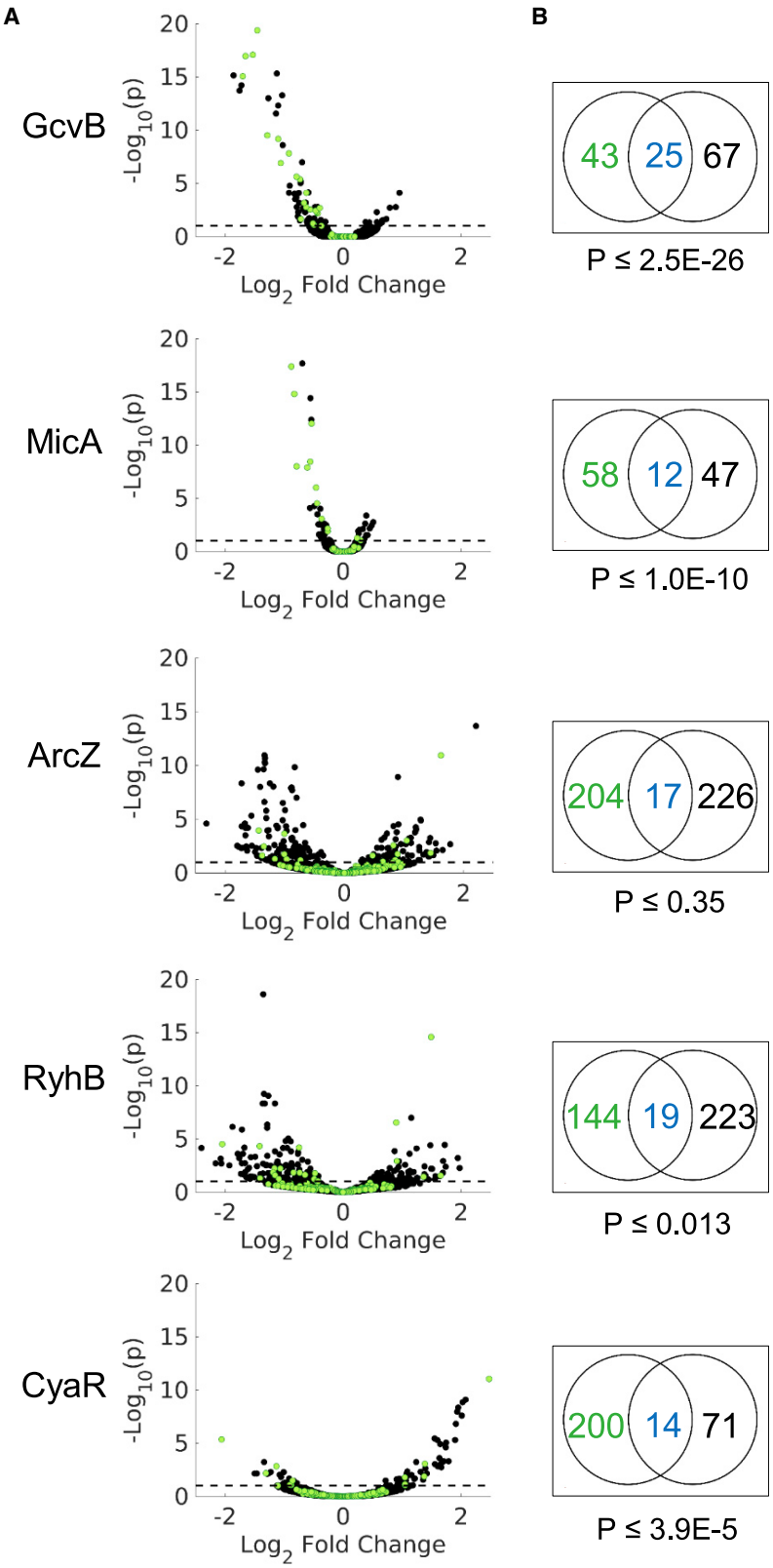

Figure 2. Measuring the Effect of the sRNA on Target mRNA Levels

(A) Only a subset of the targets shows an expression change following sRNA overexpression. Shown are Volcano plots of RNA-seq results of gene expression change following sRNA overexpression. Gene expression change is represented by the $\log_2$ fold change in expression levels, as obtained from DESeq2 analysis (Love et al., 2014) (x axis). The statistical significance of the change is represented as $-\log_{10}p$ (y axis). p is the p value corrected for multiple hypothesis testing (padj from DESeq2). For clarity, only genes with $-\log_{10}p \leq 20$ are presented. Green dots represent the sRNA targets that were detected by RIL-seq applied to *E. coli* grown to a certain growth phase or condition (GcvB to exponential phase; MicA, ArcZ, and CyaR to stationary phase; and RyhB to exponential phase under iron limitation). Black dots represent the rest of the *E. coli* genes. The dashed line represents the statistical significance threshold ($p \leq 0.1$).

(B) sRNA targets detected by RIL-seq were enriched among genes showing a statistically significant change in expression level following overexpression of the sRNA (statistical significance of the enrichment was computed by hypergeometric test). Black numbers represent non-target genes showing a statistically significant change in expression (both up- and downregulated). Blue/green numbers represent RIL-seq targets that showed/did not show a statistically significant change in expression.

See also Figures S1, S3, and S4, and Tables S1, S2, S3, and S4.

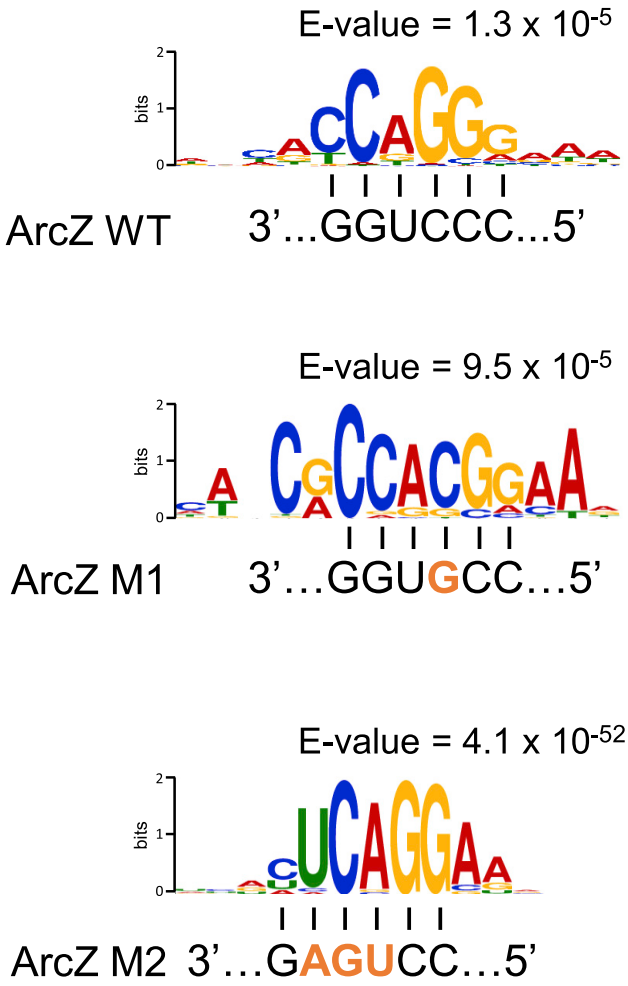

Figure 3. The sRNA Binding Site Dictates the Target Repertoire

Common motifs identified in the sequences of RIL-seq targets of ArcZ WT, ArcZ with single mutation C71G (ArcZ M1), or ArcZ with three mutations C71T T72G G73A (ArcZ M2). For each version of ArcZ, the identified common motif is complementary to the corresponding sRNA binding site sequence. The ArcZ WT sequence is shown in black, and the mutations are in orange. The motifs and E values were determined by MEME (Bailey et al., 2009). See also Figure S2 and Table S5.

and 28 targets that showed a change in their translation levels. However, we also found in the data of Wang et al., 2015 RIL-seq targets that are unaffected at both the mRNA and the translation levels, still defining a substantial subset of unaffected targets (Figure S1).

Both Affected and Unaffected Targets Are True Binders

It is important to verify that the subsets of unaffected targets do not result from false detections in the RIL-seq experiments. We previously demonstrated by sequence analysis that most sequences identified in chimeric fragments with each sRNA contained a region with sequence complementarity to the binding site of the corresponding sRNA. In addition, we showed experimentally that deletion of a major binding site of GcvB shifts the set of identified targets to targets that bind GcvB not through the major binding site but through other sites (Melamed et al., 2016). This implies that the number of false-positive sRNA interactors detected by RIL-seq is very low. To further validate RIL-seq interactions, here we assessed whether introducing a point mutation in the binding site of a sRNA instead of deleting the entire binding site shifts the target set to contain transcripts with complementary binding sites to the mutated sRNA. We tested this using the well-established sRNA ArcZ (Papenfort et al., 2009). We transformed a Δ*arcZ E. coli* strain with each of three plasmids carrying different versions of ArcZ: an ArcZ wild-type (ArcZ WT) and two mutants with substitutions in the binding site of ArcZ; a single substitution mutant, ArcZ C71G (ArcZ M1); and a mutant with three substitutions, ArcZ C71U U72G G73A (ArcZ M2). The predicted secondary structures of the RNAs encoded by the WT and both mutants, as well as their cellular levels, were similar (Figures S2A and S2B). Application of RIL-seq to these three strains identified for each of them a set of different targets (Figure S2C; Table S5). We used the MEME suite (Bailey et al., 2009) to search for a common motif in each target set. Strikingly, the best common motif in each set was complementary to the corresponding ArcZ binding site (Figure 3). These results strongly suggest that the targets identified by RIL-seq in duplexes with the sRNA are not false positives and that the sequence of the sRNA binding site dictates them. Only a fraction of the mutant ArcZ targets showed a change in expression level under overexpression of the mutant ArcZ. For the single mutation, 8% of the targets were affected (a fraction similar to ArcZ WT) (Table S3), but one-third of them were actually ArcZ WT targets, which were bound with a mismatch by the mutant sRNA. For the triple mutant, the affected targets made up only 1.5% of all targets (Table S5).

For all studied sRNAs, high fractions of the subsets of both affected and unaffected targets contain complementary sequences to the sRNA binding site (71%–100% and 64%–100% for the affected and unaffected targets, respectively) (Figure 4; Tables S3 and S4). Furthermore, we computed for each binding site its degree of conservation using a dataset of 1,118 *Enterobacteriaceae* genomic sequences and found for all sRNAs that the identified binding sites in their respective affected and unaffected target sequences showed similar degrees of evolutionary conservation (Figure S3; Table S3). Yet, the sequence conservation across *Enterobacteriaceae* genomes is high in general, so for most sRNAs it was hard to distinguish the conservation of the site from the conservation of the gene sequence in which it is embedded (Figure S3). Nevertheless, the presence of the sRNA binding site in both subsets supports the conjecture that both the affected and the unaffected targets are bound to the respective sRNA. Are there other features that differentiate between the two subsets and can explain their different responses to the sRNA? We address this question in the next sections.

The Detection of Affected Targets Is Reproducible, and They Are Involved in More Chimeric Fragments Than Unaffected Targets

Because we repeated the RIL-seq experiment several times under each studied condition (exponential phase, stationary phase, and exponential phase under iron limitation), we could examine the detection reproducibility of affected and unaffected targets.

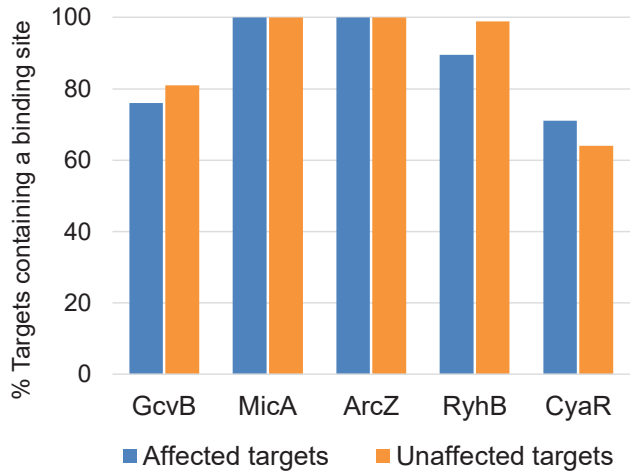

Figure 4. Both Affected and Unaffected Targets Contain a Complementary Sequence to the Binding Site of Their Interacting sRNA

A bar plot representing the percentages of affected and unaffected targets containing complementary sequences to the binding site of the respective sRNA (Melamed et al., 2016). High percentages of targets with complementary binding sites were observed for both subsets of targets. Blue and orange bars represent the affected and unaffected targets, respectively. See also Tables S3 and S4.

Each replicate experiment yielded a sequencing library, which we analyzed separately. In addition, we analyzed the results of a unified library, in which counts of sequenced fragments from the individual libraries were summed (Melamed et al., 2016). RNA-RNA pairs were determined to be putatively interacting if they passed the statistical filter in the unified library. For each interaction, we also recorded the number of individual libraries in which it was determined to be statistically significant. We treat the latter as a measure of the reproducibility of detecting an interaction and ask whether the affected and unaffected targets differed in this measure. For all sRNAs, the subsets of affected targets were identified in more replicate experiments than the subsets of unaffected targets, and these differences were statistically significant for GcvB, MicA, and ArcZ (Figure 5A; Tables S3 and S4) ($p < 0.002$ to $p < 0.04$ by Wilcoxon rank-sum test). This may suggest that the subset of affected targets per sRNA constitutes a core of steady interactions under the studied growth condition, whereas the other interactions are more sporadic.

The number of chimeric fragments for each detected sRNA-target pair in the RIL-seq experiments provides an estimate of the relative number of Hfq-mediated interactions for each pair (hereinafter, interaction frequency). Comparison of the distributions of chimeric fragment counts between the affected and the unaffected targets of each sRNA in the unified libraries revealed that the affected targets were identified in more chimeric fragments with the sRNA than the unaffected targets, and these differences were statistically significant for GcvB, MicA, ArcZ, and RyhB (Figure 5B; Table S3) ($p < 0.002$ to $p < 0.04$ by Wilcoxon rank-sum test). These results suggest that under the studied growth conditions, the affected targets show higher interaction frequency with the sRNA than do the unaffected targets.

The sRNA-Target Interaction Frequency Is Associated with the Hfq Occupancy of the Target RNA

An interaction between two biological molecules is largely determined by their binding affinity and by their concentrations. For Hfq-mediated sRNA-target interactions, the binding affinity could be reflected by the base-pairing potential between the sRNA and the target RNA, and the relevant concentrations could be reflected by the amounts of the Hfq-bound sRNA and the Hfq-bound target. Although the explicit values of these measures are unavailable, we can obtain coarse estimations for the binding capabilities by computing the binding free energy of the sRNA-target duplex and coarse estimations for the amounts of Hfq-bound RNAs from the read counts of the RIL-seq experiments (for this, the unified libraries were considered). We compute these measures for each interaction of a studied sRNA and examine whether there is a correlation between each of these measures and the number of chimeric fragments.

Although we found that both affected and unaffected targets harbor binding sites for the respective sRNAs, they can still differ in the free energy of binding. We computed the free energy of binding by two tools: RNAduplex, by which we computed explicitly the free energy of the duplex made between the known sRNA binding site and the predicted target binding site, and RNAup, which also considers predicted secondary structures that need to be unfolded to make the duplex (STAR Methods). Our results indicate only a weak correlation between the binding free energy of the sRNA-target duplex and the number of chimeric fragments (Figure 6A; Table S3). This result was independent of the method used for computing the binding free energy. Of note, there was no difference between affected and unaffected targets in the binding site location within the mRNA. Most putative binding sites of the sRNAs were located within the coding sequence of the targets, except for GcvB, for which the putative binding sites were mostly identified in the 5′ UTR (Table S4).

The abundances of the Hfq-bound sRNA and Hfq-bound target transcript are reflected by their corresponding RNA sequencing (RNA-seq) read counts in immunoprecipitation experiments of Hfq (hereinafter, $sRNA_{Hfq}$ abundance and $target_{Hfq}$ abundance). We obtained these counts from the number of sequencing reads covering the sRNA and the target transcript regions captured in the RIL-seq experiments, including both chimeric and non-chimeric fragments (single fragments). Because we analyzed the targets of each sRNA separately, we could treat the value of $sRNA_{Hfq}$ abundance as constant and assess the correlation between the number of chimeric fragments and the $target_{Hfq}$ abundance. As shown in Figure 6B, for all studied sRNAs we observed a high correlation between the numbers of chimeric fragments and the $target_{Hfq}$ abundances ($0.82 \leq r \leq 0.95$, $p < 10^{-51}$ to $p < 10^{-16}$), implying an association between the $target_{Hfq}$ abundance and the sRNA-target interaction frequency. To control for possible indirect effects due to differences in the expression levels of the targets, we also computed the partial correlation between the $target_{Hfq}$ abundance and the number of chimeric fragments while controlling for the effect of the expression levels of the genes. The latter were obtained from RNA-seq analyses performed for RNA extracted from the same cell lysates that were used for the RIL-seq experiments in Melamed et al. (2016). The region for which

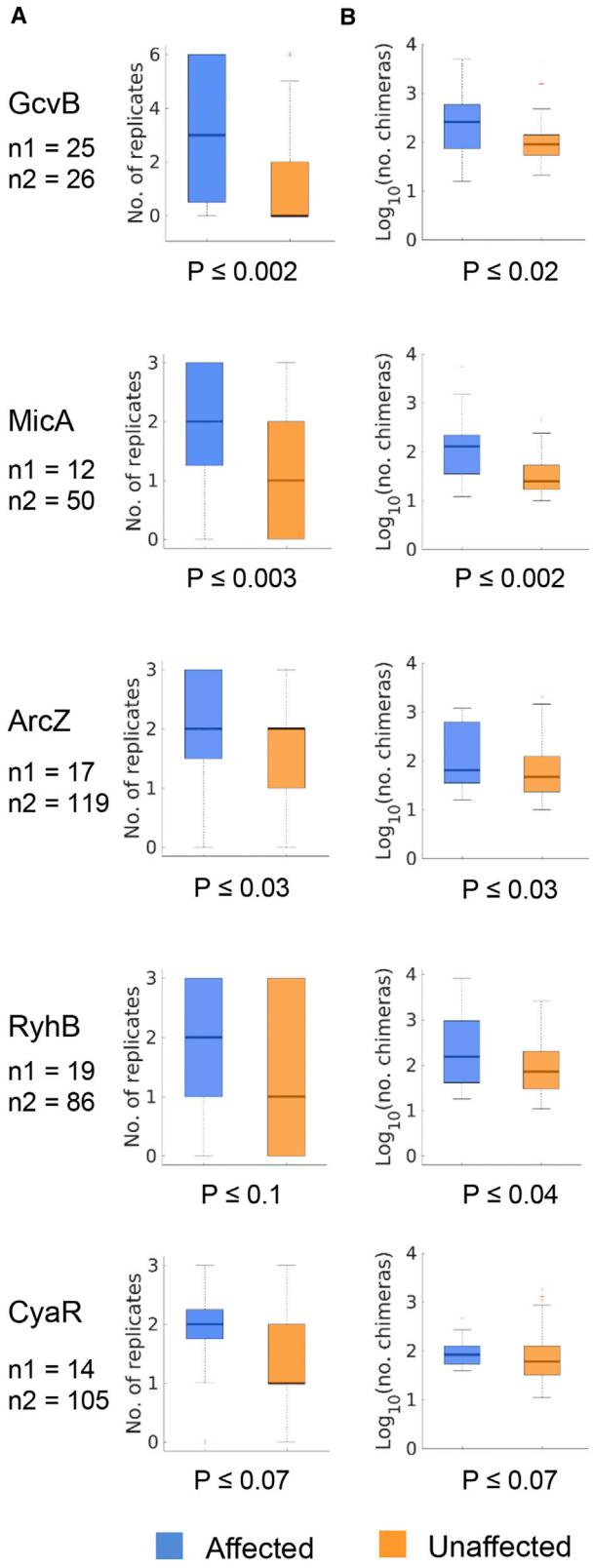

Figure 5. The Interactions of the sRNA with Affected Targets Are Reproducibly Detected and Are More Abundant Than the Interactions with Unaffected Targets

(A) Interactions with affected targets were identified in more replicate experiments than interactions with unaffected targets. A zero number of replicates represents interactions that were identified only in a unified library (i.e., unifying the results from all replicate experiments) (Melamed et al., 2016). The RIL-seq experiment included six, three, and three replicates for the exponential phase, stationary phase, and exponential phase under iron limitation, respectively. The RNA-seq experiment of GcvB was performed in the exponential phase; those of MicA, ArcZ, and CyaR were performed in the stationary phase; and that of RyhB was performed in the exponential phase under iron limitation.

(B) Affected targets establish more interactions with the sRNA than do unaffected targets, as represented by the number of chimeric fragments (log_{10}). Blue and orange colors represent the affected and unaffected targets, respectively. For each sRNA, n1 and n2 are the numbers of affected and unaffected targets, respectively. Statistical significance was assessed by Wilcoxon rank-sum test. See also Tables S3 and S4.

read coverage was used to represent the total RNA expression level corresponded to the target region included in the RIL-seq chimeric fragment. The correlation coefficient was only moderately affected by controlling for total RNA ($0.78 \leq r \leq 0.95$, $p < 10^{-41}$ to $p < 10^{-13}$), indicating that the correlation of the $target_{Hfq}$ abundance and the Hfq-mediated sRNA-target interaction frequency is independent of the expression levels of the genes. Altogether, these results strongly support the conjecture that the binding efficiency of a target RNA to Hfq plays a role in the regulatory outcome.

Not All Targets with High Hfq Occupancy Are Affected by the sRNA

Although our analyses imply an association between affected targets and their detection reproducibility and/or number of chimeric fragments, there were exceptions. On the one hand, some affected targets were discovered in only one experiment and were included in a rather small number of chimeric fragments. On the other hand, some unaffected targets were repeatedly discovered in all replicate experiments and were involved in thousands of chimeric fragments (Table S4). It is possible that the latter regard targets that exhibit a change in expression only at the protein level or that in these cases, the mRNA affects the sRNA and leads to its degradation, as was demonstrated for ChiX-*chb* interaction (Figueroa-Bossi et al., 2009; Overgaard et al., 2009). To explore these possibilities, we studied four interactions that were repeatedly revealed in multiple libraries and identified with high numbers of chimeric fragments: RyhB-*lpp*, CyaR-*lpp*, GcvB-*raiA*, and GcvB-*gatY* (Table S4). To test the possible effect of the sRNAs on the targets' translation, we constructed strains carrying a plasmid with a translational fusion of *gfp* to the target mRNA. We compared the GFP intensity in strains overexpressing the sRNA and a control strain and observed a decrease in the GFP intensity of *gatY-gfp* fusion, indicating that the negative regulation of *gatY* by GcvB is evident only at the translation level (Figure S4A). There was only a slight change in the GFP intensity of *lpp-gfp* translational fusion when overexpressing CyaR or RyhB and no change in the GFP intensity of *raiA-gfp* translational fusion when overexpressing GcvB, suggesting that these interactions do not enforce a change at the translational level (Figure S4A). To test the possible effect of the target mRNA on the sRNA, we applied

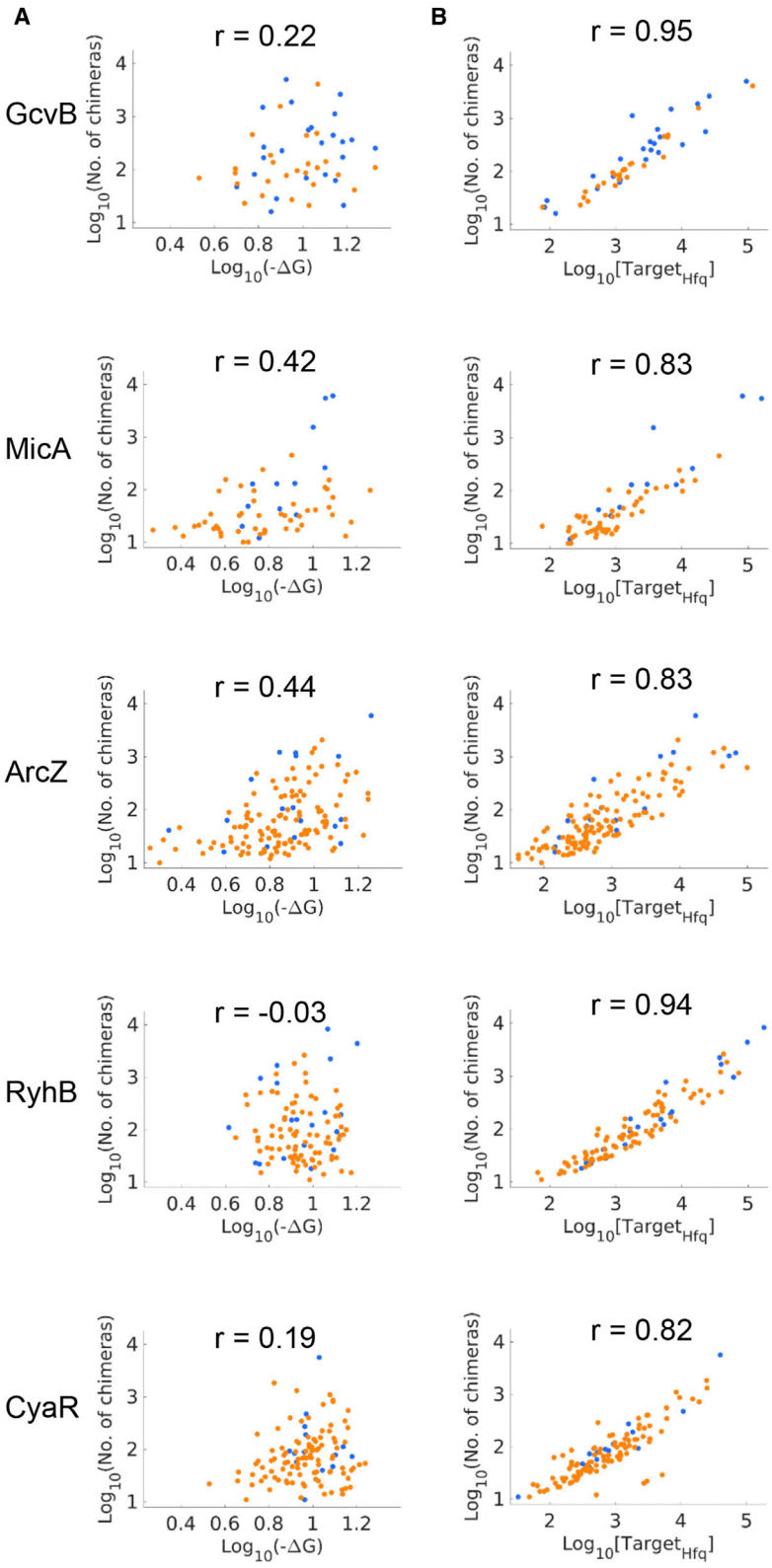

Figure 6. The Hfq Occupancy of Targets Correlates with Their Interaction Frequency

(A) The predicted binding free energy of the duplex between the target and the sRNA is only weakly correlated with the sRNA-target interaction frequency (represented by the number of chimeric fragments). Binding free energy values (in kilocalories per mole) between two interacting RNAs were computed by RNAup (Mückstein et al., 2006). Spearman correlations coefficients are presented ($p < 10^{-6}$ to $p < 0.8$).

(B) The target's Hfq occupancy is highly correlated with the sRNA-target interaction frequency. Presented is the correlation between the Hfq-target abundance ($target_{Hfq}$, number of sequenced fragments representing the target abundance on Hfq) and the number of chimeric fragments. Numbers of sequenced fragments are presented by log_{10}. Spearman correlation coefficients are presented ($p < 10^{-51}$ to $p < 10^{-16}$).

Blue and orange dots represent the affected and unaffected targets, respectively. See also Tables S3 and S4.

northern blot analysis but observed no change in the sRNA level for RyhB-*lpp*, CyaR-*lpp*, and GcvB-*raiA* interactions (Figures S4B and S4C). Recently, it was shown in *Salmonella* that the 3′ UTR of *raiA* encodes a sRNA named RaiZ (Smirnov et al., 2017). RaiZ was also detected in *E. coli* in the RIL-seq experiment (see Table S2 in Melamed et al., 2016). To rule out the possible effect of GcvB-*raiA* interaction on RaiZ levels and of RaiZ on GcvB levels, we tested whether overexpression of RaiZ affects GcvB, and vice versa. However, no such effect was observed (Figures S4C and S4D). These results suggest that in some steady interactions for which no effect on the target RNA level was detected, the regulation might be manifested at the target protein level, as found for *gatY*. Still, other steady interactions do not lead to changes at either the target RNA or the protein level, suggesting that some steady sRNA-target interactions possibly have other roles yet to be revealed.

DISCUSSION

In this study, we attempted to gain insights into the underlying principles of Hfq-mediated regulation by sRNA through the combination of gene expression data under overexpression of a sRNA and *in vivo* sRNA-target interaction data determined by RIL-seq (Melamed et al., 2016, 2018; Figure 1). Although previous studies used sequence complementarity considerations and/or gene expression changes as proxies for defining sRNA targets, RIL-seq provides objective and unbiased data of sRNA-target pairs, enabling the assessment of these target properties rather than their use as defining attributes. First, because RIL-seq provides information on direct sRNA-target duplexes, it opens the door for characterization of the sequences bound to the sRNA using direct rather than indirect information. Previously, such analyses were carried out on data of genes that changed their expression following overexpression of a sRNA or a microRNA (miRNA) (e.g., Fröhlich et al., 2016; Lim et al., 2005), which possibly included secondary, indirect targets. Our results demonstrate that the target binding site on the sRNA dictates the repertoire of targets found in duplexes with the sRNA (Figure 3), consistent with our previous result, which found that for all target sets, the best common sequence motif is the one that complements the binding site on the sRNA (Melamed et al., 2016). Furthermore, we provide the first direct evidence that changing one or a few nucleotides in the binding site harbored in the sRNA sequence shifts the repertoire of bound targets to include sequences that exhibit complementarity to the mutated binding site (Figure 3). Second, we can assess whether the sRNA affects the expression levels of the identified targets as expected. Surprisingly, by comparing RNA-seq results between a strain overexpressing a studied sRNA and a control strain, we observed that only a subset of targets of the corresponding sRNA was affected at the transcript expression levels under the studied conditions, whereas other targets were unaffected. We obtained a similar classification of targets into affected and unaffected subsets using recent interaction data in *E. coli* published by Melamed et al. (2020).

The affected targets were repeatedly discovered in duplexes with the sRNA in replicate experiments, whereas most duplexes involving unaffected targets were discovered only in the unified library. In addition, the affected targets showed higher interaction frequency with the sRNA (represented by the number of chimeric fragments) than the unaffected ones. Altogether, our results suggest that under a studied condition, the sRNA influences the expression levels of a core of targets involved in steady interactions, whereas other targets interact with the sRNA more sporadically and the sRNA barely affects their expression levels.

For most sRNA-target interactions to be fulfilled, the target has to be bound to Hfq and has to base pair with the sRNA. Thus, the differences in the frequencies of sRNA-target interaction among various targets could be reflected in the variability in Hfq binding and/or in the variability in sRNA base-pairing capabilities across the various targets. Our results indicate that both affected and unaffected targets contain the binding motif to the sRNA. In addition, using the available tools for assessing the binding free energy of the sRNA-target duplex, we found only a weak correlation between this attribute and the interaction frequency (Figure 6A). These results imply that differences in base-pairing capability to the sRNA do not play a major role in determining the differences in the interaction frequency and hence in the outcome of the sRNA-target interaction. Yet because the available methods for evaluating the free energy of binding of two RNAs do not take into account possible structural re-arrangements due to protein binding (Santiago-Frangos and Woodson, 2018; Wroblewska and Olejniczak, 2016), the preceding conclusion should be re-assessed when improved RNA structure predictive algorithms become available. As to the target-Hfq binding attribute, our results indicated a high correlation between the sRNA-target interaction frequency and the Hfq occupancy of the targets under the studied condition (Figure 6B), alluding to a higher Hfq binding efficiency of the targets involved in many interactions with the sRNA, most of which belong to the set of affected targets. Because the cellular concentration of Hfq is maintained within a limited range due to its tight autoregulation (Morita and Aiba, 2019), there is competition among RNAs over binding to Hfq. Moreover, there is continuous cycling of RNAs on Hfq (Fender et al., 2010; Wagner, 2013), which also implies that more efficient Hfq binders might have an advantage.

Previous studies mainly focused on the competition among sRNAs (Kwiatkowska et al., 2018; Moon and Gottesman, 2011; Olejniczak, 2011) or on the balance between the amounts of bound sRNA and mRNA (Hussein and Lim, 2011). The importance of efficient Hfq binding of the target to the regulation outcome was demonstrated experimentally by Beisel et al. (2012), who studied the effect of the sRNA Spot42 on its various targets. Previous theoretical analyses that addressed the regulatory outcome of sRNA-target interaction have not considered the efficiency of Hfq-target binding (Levine and Hwa, 2008; Mehta et al., 2008; Shimoni et al., 2007). These studies suggested that sRNAs establish a linear threshold for their target gene expression. The expression of a target is regulated as long as its transcription rate is lower than the transcription rate of its regulating sRNA; once the transcription rate of the target exceeds that of the sRNA, the regulatory effect depends on the difference in the transcription rates of the target and sRNA (Levine and Hwa, 2008). Our results suggest that these considerations might have been incomplete, because they did not consider the prerequisite of target-Hfq binding for the regulation to take

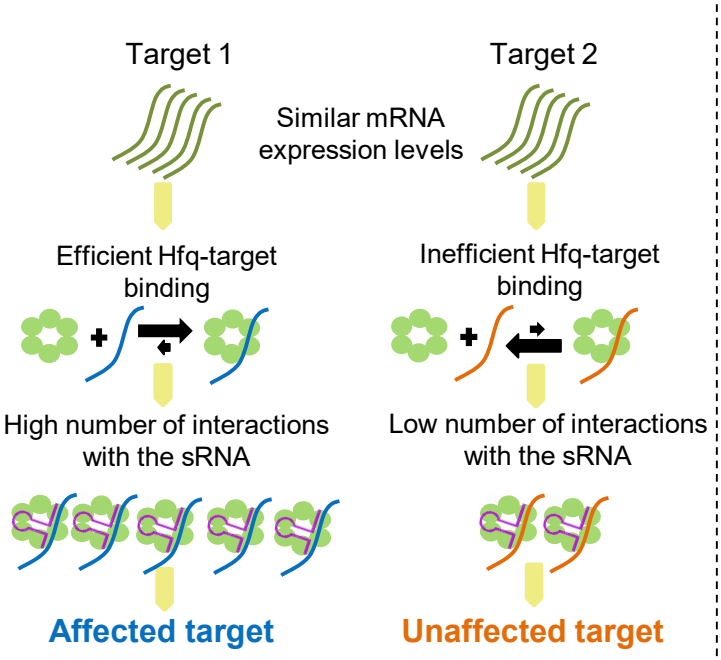

Figure 7. The Binding Efficiency of a Target Transcript to Hfq Affects Its Regulatory Fate

Competition between targets over binding to Hfq is a major determinant of the regulatory fate of the targets. Left panel: a target that binds Hfq efficiently will compete successfully with other targets over binding to Hfq, resulting in more interactions with the sRNA and a change in expression. Right panel: a target that is an inefficient Hfq binder will not succeed in competing with other targets over binding to Hfq, resulting in a low number of sRNA-target interactions and no effect on the expression level of the target. Green circles represent Hfq monomers. Green, blue, and orange waved lines represent a target RNA, an affected target RNA, and an unaffected target RNA, respectively. The sRNA is depicted in purple.

place. For example, *sstT* and *cysB* are two GcvB targets identified by RIL-seq that are comparable in their expression levels in the exponential phase and in their predicted binding free energy to GcvB (Table S4). We use the total expression level as an estimation of the transcription rate, because it was shown that these values are highly correlated (Chen et al., 2015). Yet the $sstT_{Hfq}$ abundance is much higher (119,491 reads) than the $cysB_{Hfq}$ abundance (538 reads). This is manifested in the RIL-seq experiment in a high number of chimeric fragments of GcvB with *sstT* (17,893 reads) and a low number of chimeric fragments with *cysB* (52 reads). Consistently, there is a statistically significant downregulation of *sstT* by GcvB and no change in the mRNA level of *cysB* by GcvB. Thus, even though the two targets are similar in their total expression levels and in their predicted free energy upon binding to GcvB, they are affected differently by the sRNA, apparently because of the difference in their Hfq binding. Hence, a target gene may have a lower transcription rate than the sRNA, but without efficiently binding the Hfq, its regulation by the sRNA might be minimal. Weak Hfq binding and thus low Hfq occupancy would conceivably result in a low interaction frequency with no effect on the target level (Figure 7). Thus, efficient Hfq binding would probably award that target an advantage in the competition with other targets in the cycling process and over binding to the sRNA, resulting in a relatively high interaction frequency, which is evident in an expression change.

It is conceivable that affected targets contain a binding motif that allows their binding to the respective Hfq face, consistent with the class of their regulating sRNA (Schu et al., 2015). The Hfq hexamer contains three distinct RNA binding surfaces—proximal face, rim, and distal face—that facilitate regulation by sRNAs. The proximal face binds uridine-rich sequences; the distal face binds ARN-, ARNN-, or AAN-rich sequences (A, adenine nucleotide; R, purine nucleotide; N, any nucleotide); and the rim binds UA-rich (U, uridine nucleotide) sequences (Dimastrogiovanni et al., 2014; Link et al., 2009; Mikulecky et al., 2004; Schumacher et al., 2002; Zhang et al., 2013). The sRNAs are classified into two classes by the Hfq face they bind. Class I sRNAs bind the proximal face through a U-rich RNA sequence and the rim through a UA binding motif. The targets that are regulated by class I sRNAs contain ARN- or AAN-rich sequences and interact with the distal face of Hfq. Class II sRNAs contain a U-rich sequence for binding the Hfq proximal face and an ARN-rich sequence motif for binding the distal face. The targets that are regulated by class II sRNAs contain a UA motif and bind the rim of Hfq (Schu et al., 2015). Conceivably, targets that contain the corresponding class I/II Hfq binding motif will bind Hfq efficiently and undergo more efficient regulation by the sRNA. However, we did not identify an enrichment of an ARN binding motif in the sequences of affected targets of the class I sRNAs (GcvB, MicA, ArcZ, and RyhB) or a UA-rich motif in targets of CyaR, classified as a class II sRNA. This finding is consistent with a previous study by Holmqvist et al. (2016), who also could not identify an ARN binding motif in Hfq-bound mRNAs. Thus, the differences in Hfq binding might result from more complex features, combining sequence and structure considerations.

Taking the competition over binding to Hfq into account raises the possibility that the definition of affected and unaffected targets of a sRNA may be condition dependent, because the repertoire of Hfq binding competitors can change in various growth conditions. In one scenario, a target with a high Hfq binding efficiency that is expressed under a certain condition can be lowly expressed in another condition, freeing some Hfq proteins for binding other targets, possibly with weaker Hfq binding efficiencies. This can lead to stronger regulation by the sRNA of targets that are relatively weak Hfq binders. In another scenario, a target that was not expressed under a certain condition can increase in expression and in Hfq binding under another condition, occupying the Hfq and preventing other targets from being affected. This scenario was exemplified in several studies (Figueroa-Bossi et al., 2009; Lalaouna et al., 2015; Miyakoshi

et al., 2015; Overgaard et al., 2009). In addition, it is possible that under other conditions, the structure of the target RNA may change, leading to a change in its Hfq binding efficiency. This can explain why, for example, some known ArcZ targets were not affected at the tested growth condition in this study but were affected in other growth conditions tested in previous studies (*sdaC* and *tpx* in Papenfort et al., 2009 and *flhD* in De Lay and Gottesman, 2012).

Although the competition over binding to Hfq provides a plausible explanation to the lack of expression change of the unaffected targets, there might be other explanations for some unaffected targets, either technical or biological. Possible technical explanations include the following: (1) Targets might be lowly expressed and would have been identified as affected once the sequencing depth is increased. This is due to the limitations of a large-scale methodology, in which the detection of expression change depends on the depth of the RNA-seq libraries. Finding a statistically significant change for lowly expressed genes is difficult, because high noise may mask biological effects. (2) Genes might be misclassified as targets by RIL-seq. Although the statistical analysis of RIL-seq data was designed to minimize the capturing of spurious interactions, some may have escaped our statistical filtering. Possible biological explanations include the following: (1) Targets might be affected at the protein level, but not at the RNA level, as demonstrated here for GcvB-*gatY* interaction (Figure S4A) and for various RyhB interactions by Wang et al. (2015). Similar examples were reported for miRNAs (Stern-Ginossar et al., 2007). (2) Targets might interact with the sRNA to accomplish a task different from the regulation of their own expression level. For example, two studies suggested that the unaffected sRNA targets could act as competitive inhibitors of the affected targets (Jost et al., 2013; Seitz, 2009). These studies classified the targets of regulatory RNAs into primary and auxiliary targets, for which only the regulation of primary targets has a phenotypic effect. The auxiliary targets were conjectured as competitive inhibitors of the regulatory RNAs, maintaining their binding to the affected targets at the desired level, reducing noise, and conferring robustness to their regulation (Jost et al., 2013; Seitz, 2009). (3) Some targets that did not show a statistically significant change in expression may undergo only mild fine-tuning by the sRNA. It is also interesting that some affected targets, which showed a statistically significant expression change, exhibited a change of less than two-fold. These results are consistent with studies in the miRNA field, in which modest changes in gene expression were observed for many miRNA targets (Baek et al., 2008; Selbach et al., 2008), suggesting that one of the major roles of regulation by non-coding RNAs is to fine-tune gene expression.

In principle, two types of competition among targets are predicted to influence the regulatory outcome: competition over binding to the Hfq protein and competition over base pairing with the Hfq-bound sRNA. However, because our results suggest that the competition over base pairing with the sRNA is mostly determined by the Hfq occupancy of the different targets, it appears that binding efficiency of the target to Hfq actually affects the two types of competition and plays a major role in the regulatory outcome. What underlies the difference in Hfq binding among the various targets has yet to be revealed.

STAR★METHODS

Detailed methods are provided in the online version of this paper and include the following:

- KEY RESOURCES TABLE
- LEAD CONTACT AND MATERIALS AVAILABILITY
- EXPERIMENTAL MODEL AND SUBJECT DETAILS
- METHOD DETAILS
  - Plasmid construction
  - Bacterial strains used in RNA-seq experiments
  - Culture conditions for RNA-seq experiments
  - RNA extraction
  - RNA sequencing
  - Northern analysis
  - GFP reporter assay
- QUANTIFICATION AND STATISTICAL ANALYSIS
  - Differential expression analysis using DESeq2
  - Wilcoxon rank sum test, Hypergeometric test, Spearman correlation and Spearman partial correlation
  - Identification of a common motif in the target sets
  - Prediction of RNA secondary structure
  - Sequence conservation analysis of binding sites
  - Binding free energy computation
- DATA AND CODE AVAILABILITY

SUPPLEMENTAL INFORMATION

Supplemental Information can be found online at https://doi.org/10.1016/j.celrep.2020.02.016.

ACKNOWLEDGMENTS

This study was supported by the European Research Council (Advanced Grants 322920 and 833598), I-CORE Programs of the Planning and Budgeting Committee and The Israel Science Foundation (grants 1796/12 and 41/1), and the Israel Science Foundation administered by the Israeli Academy for Sciences and Humanities (grant 876/17). Y.E.G. was partially supported by the Hoffman Foundation. We thank T. Bamberger, D. Rabinovich, and M. Kournos for technical help; Y. Altuvia for fruitful discussions; E. Romm for graphical help; and S. Altuvia, A. Peer, S.P. Mizrahi, A. Bar, and M. Nitzan for helpful advice.

AUTHOR CONTRIBUTIONS

Experimental Investigation, R.F.-R., M.B., and L.A.; Computational Analysis, R.F.-R., A.R., and Y.E.G.; Writing – Original Draft, R.F.-R. and H.M.; Writing – Review & Editing, R.F.-R., L.A., A.R., Y.E.G., M.B., and H.M.; Supervision, H.M.

DECLARATION OF INTERESTS

The authors declare no competing interests.

Received: August 22, 2019
Revised: January 15, 2020
Accepted: February 4, 2020
Published: March 3, 2020

REFERENCES

Argaman, L., Hershberg, R., Vogel, J., Bejerano, G., Wagner, E.G., Margalit, H., and Altuvia, S. (2001). Novel small RNA-encoding genes in the intergenic regions of *Escherichia coli*. Curr. Biol. *11*, 941–950.

Baba, T., Ara, T., Hasegawa, M., Takai, Y., Okumura, Y., Baba, M., Datsenko, K.A., Tomita, M., Wanner, B.L., and Mori, H. (2006). Construction of Escherichia coli K-12 in-frame, single-gene knockout mutants: the Keio collection. Mol. Syst. Biol. 2006.0008. https://doi.org/10.1038/msb4100050.

Baek, D., Villén, J., Shin, C., Camargo, F.D., Gygi, S.P., and Bartel, D.P. (2008). The impact of microRNAs on protein output. Nature *455*, 64–71.

Bailey, T.L., Boden, M., Buske, F.A., Frith, M., Grant, C.E., Clementi, L., Ren, J., Li, W.W., and Noble, W.S. (2009). MEME SUITE: tools for motif discovery and searching. Nucleic Acids Res. *37*, W202–W208.

Beisel, C.L., Updegrove, T.B., Janson, B.J., and Storz, G. (2012). Multiple factors dictate target selection by Hfq-binding small RNAs. EMBO J. *31*, 1961–1974.

Camacho, C., Coulouris, G., Avagyan, V., Ma, N., Papadopoulos, J., Bealer, K., and Madden, T.L. (2009). BLAST+: architecture and applications. BMC Bioinformatics *10*, 421.

Chen, H., Shiroguchi, K., Ge, H., and Xie, X.S. (2015). Genome-wide study of mRNA degradation and transcript elongation in *Escherichia coli*. Mol. Syst. Biol. *11*, 781.

Cock, P.J., Antao, T., Chang, J.T., Chapman, B.A., Cox, C.J., Dalke, A., Friedberg, I., Hamelryck, T., Kauff, F., Wilczynski, B., and de Hoon, M.J. (2009). Biopython: freely available Python tools for computational molecular biology and bioinformatics. Bioinformatics *25*, 1422–1423.

Coornaert, A., Lu, A., Mandin, P., Springer, M., Gottesman, S., and Guillier, M. (2010). MicA sRNA links the PhoP regulon to cell envelope stress. Mol. Microbiol. *76*, 467–479.

Corcoran, C.P., Podkaminski, D., Papenfort, K., Urban, J.H., Hinton, J.C., and Vogel, J. (2012). Superfolder GFP reporters validate diverse new mRNA targets of the classic porin regulator, MicF RNA. Mol. Microbiol. *84*, 428–445.

Datsenko, K.A., and Wanner, B.L. (2000). One-step inactivation of chromosomal genes in *Escherichia coli* K-12 using PCR products. Proc. Natl. Acad. Sci. USA *97*, 6640–6645.

De Lay, N., and Gottesman, S. (2009). The Crp-activated small noncoding regulatory RNA CyaR (RyeE) links nutritional status to group behavior. J. Bacteriol. *191*, 461–476.

De Lay, N., and Gottesman, S. (2012). A complex network of small non-coding RNAs regulate motility in *Escherichia coli*. Mol. Microbiol. *86*, 524–538.

Dimastrogiovanni, D., Fröhlich, K.S., Bandyra, K.J., Bruce, H.A., Hohensee, S., Vogel, J., and Luisi, B.F. (2014). Recognition of the small regulatory RNA RydC by the bacterial Hfq protein. eLife *3*, e05375.

Edgar, R.C. (2004). MUSCLE: multiple sequence alignment with high accuracy and high throughput. Nucleic Acids Res. *32*, 1792–1797.

Fender, A., Elf, J., Hampel, K., Zimmermann, B., and Wagner, E.G. (2010). RNAs actively cycle on the Sm-like protein Hfq. Genes Dev. *24*, 2621–2626.

Figueroa-Bossi, N., Valentini, M., Malleret, L., Fiorini, F., and Bossi, L. (2009). Caught at its own game: regulatory small RNA inactivated by an inducible transcript mimicking its target. Genes Dev. *23*, 2004–2015.

Fröhlich, K.S., Haneke, K., Papenfort, K., and Vogel, J. (2016). The target spectrum of SdsR small RNA in Salmonella. Nucleic Acids Res. *44*, 10406–10422.

Groszewska, A., Wroblewska, Z., and Olejniczak, M. (2016). The structure of fadL mRNA and its interactions with RybB sRNA. Acta Biochim. Pol. *63*, 835–840.

Holmqvist, E., Wright, P.R., Li, L., Bischler, T., Barquist, L., Reinhardt, R., Backofen, R., and Vogel, J. (2016). Global RNA recognition patterns of post-transcriptional regulators Hfq and CsrA revealed by UV crosslinking *in vivo*. EMBO J. *35*, 991–1011.

Hör, J., Gorski, S.A., and Vogel, J. (2018). Bacterial RNA Biology on a Genome Scale. Mol. Cell *70*, 785–799.

Hussein, R., and Lim, H.N. (2011). Disruption of small RNA signaling caused by competition for Hfq. Proc. Natl. Acad. Sci. USA *108*, 1110–1115.

Jacques, J.F., Jang, S., Prévost, K., Desnoyers, G., Desmarais, M., Imlay, J., and Massé, E. (2006). RyhB small RNA modulates the free intracellular iron pool and is essential for normal growth during iron limitation in *Escherichia coli*. Mol. Microbiol. *62*, 1181–1190.

Jost, D., Nowojewski, A., and Levine, E. (2013). Regulating the many to benefit the few: role of weak small RNA targets. Biophys. J. *104*, 1773–1782.

Kery, M.B., Feldman, M., Livny, J., and Tjaden, B. (2014). TargetRNA2: identifying targets of small regulatory RNAs in bacteria. Nucleic Acids Res. *42*, W124–W129.

Kim, S. (2015). ppcor: An R Package for a Fast Calculation to Semi-partial Correlation Coefficients. Commun. Stat. Appl. Methods *22*, 665–674.

Kwiatkowska, J., Wroblewska, Z., Johnson, K.A., and Olejniczak, M. (2018). The binding of Class II sRNA MgrR to two different sites on matchmaker protein Hfq enables efficient competition for Hfq and annealing to regulated mRNAs. RNA *24*, 1761–1784.

Lalaouna, D., Carrier, M.C., Semsey, S., Brouard, J.S., Wang, J., Wade, J.T., and Massé, E. (2015). A 3′ external transcribed spacer in a tRNA transcript acts as a sponge for small RNAs to prevent transcriptional noise. Mol. Cell *58*, 393–405.

Levine, E., and Hwa, T. (2008). Small RNAs establish gene expression thresholds. Curr. Opin. Microbiol. *11*, 574–579.

Li, H. (2013). Aligning sequence reads, clone sequences and assembly contigs with BWA-MEM. arXiv, arXiv:1303.3997v2. https://arxiv.org/abs/1303.3997.

Lim, L.P., Lau, N.C., Garrett-Engele, P., Grimson, A., Schelter, J.M., Castle, J., Bartel, D.P., Linsley, P.S., and Johnson, J.M. (2005). Microarray analysis shows that some microRNAs downregulate large numbers of target mRNAs. Nature *433*, 769–773.

Link, T.M., Valentin-Hansen, P., and Brennan, R.G. (2009). Structure of *Escherichia coli* Hfq bound to polyriboadenylate RNA. Proc. Natl. Acad. Sci. USA *106*, 19292–19297.

Lorenz, R., Bernhart, S.H., Höner Zu Siederdissen, C., Tafer, H., Flamm, C., Stadler, P.F., and Hofacker, I.L. (2011). ViennaRNA Package 2.0. Algorithms Mol. Biol. *6*, 26.

Love, M.I., Huber, W., and Anders, S. (2014). Moderated estimation of fold change and dispersion for RNA-seq data with DESeq2. Genome Biol. *15*, 550.

Martin, M. (2011). Cutadapt removes adapter sequences from high-throughput sequencing reads. EMBnet J. *17*, 10–12.

Mehta, P., Goyal, S., and Wingreen, N.S. (2008). A quantitative comparison of sRNA-based and protein-based gene regulation. Mol. Syst. Biol. *4*, 221.

Melamed, S., Peer, A., Faigenbaum-Romm, R., Gatt, Y.E., Reiss, N., Bar, A., Altuvia, Y., Argaman, L., and Margalit, H. (2016). Global Mapping of Small RNA-Target Interactions in Bacteria. Mol. Cell *63*, 884–897.

Melamed, S., Faigenbaum-Romm, R., Peer, A., Reiss, N., Shechter, O., Bar, A., Altuvia, Y., Argaman, L., and Margalit, H. (2018). Mapping the small RNA interactome in bacteria using RIL-seq. Nat. Protoc. *13*, 1–33.

Melamed, S., Adams, P.P., Zhang, A., Zhang, H., and Storz, G. (2020).). RNA-RNA Interactomes of ProQ and Hfq Reveal Overlapping and Competing Roles. Mol. Cell *77*, 411–425.

Mikulecky, P.J., Kaw, M.K., Brescia, C.C., Takach, J.C., Sledjeski, D.D., and Feig, A.L. (2004). *Escherichia coli* Hfq has distinct interaction surfaces for DsrA, rpoS and poly(A) RNAs. Nat. Struct. Mol. Biol. *11*, 1206–1214.

Miyakoshi, M., Chao, Y., and Vogel, J. (2015). Cross talk between ABC transporter mRNAs via a target mRNA-derived sponge of the GcvB small RNA. EMBO J. *34*, 1478–1492.

Moon, K., and Gottesman, S. (2011). Competition among Hfq-binding small RNAs in *Escherichia coli*. Mol. Microbiol. *82*, 1545–1562.

Morita, T., and Aiba, H. (2019). Mechanism and physiological significance of autoregulation of the *Escherichia coli hfq* gene. RNA *25*, 264–276.

Mückstein, U., Tafer, H., Hackermüller, J., Bernhart, S.H., Stadler, P.F., and Hofacker, I.L. (2006). Thermodynamics of RNA-RNA binding. Bioinformatics *22*, 1177–1182.

O'Leary, N.A., Wright, M.W., Brister, J.R., Ciufo, S., Haddad, D., McVeigh, R., Rajput, B., Robbertse, B., Smith-White, B., Ako-Adjei, D., et al. (2016).

Reference sequence (RefSeq) database at NCBI: current status, taxonomic expansion, and functional annotation. Nucleic Acids Res. *44* (*D1*), D733–D745.

Olejniczak, M. (2011). Despite similar binding to the Hfq protein regulatory RNAs widely differ in their competition performance. Biochemistry *50*, 4427–4440.

Overgaard, M., Johansen, J., Møller-Jensen, J., and Valentin-Hansen, P. (2009). Switching off small RNA regulation with trap-mRNA. Mol. Microbiol. *73*, 790–800.

Papenfort, K., Said, N., Welsink, T., Lucchini, S., Hinton, J.C.D., and Vogel, J. (2009). Specific and pleiotropic patterns of mRNA regulation by ArcZ, a conserved, Hfq-dependent small RNA. Mol. Microbiol. *74*, 139–158.

R Core Team (2017). R: A language and environment for statistical computing (R Foundation for Statistical Computing).

Santiago-Frangos, A., and Woodson, S.A. (2018). Hfq chaperone brings speed dating to bacterial sRNA. Wiley Interdiscip. Rev. RNA *9*, e1475.

Santos-Zavaleta, A., Salgado, H., Gama-Castro, S., Sánchez-Pérez, M., Gómez-Romero, L., Ledezma-Tejeida, D., García-Sotelo, J.S., Alquicira-Hernández, K., Muñiz-Rascado, L.J., Peña-Loredo, P., et al. (2019). RegulonDB v 10.5: tackling challenges to unify classic and high throughput knowledge of gene regulation in *E. coli* K-12. Nucleic Acids Res. *47* (*D1*), D212–D220.

Schneider, T.D., and Stephens, R.M. (1990). Sequence logos: a new way to display consensus sequences. Nucleic Acids Res. *18*, 6097–6100.

Schneider, T.D., Stormo, G.D., Gold, L., and Ehrenfeucht, A. (1986). Information content of binding sites on nucleotide sequences. J. Mol. Biol. *188*, 415–431.

Schu, D.J., Zhang, A., Gottesman, S., and Storz, G. (2015). Alternative Hfq-sRNA interaction modes dictate alternative mRNA recognition. EMBO J. *34*, 2557–2573.

Schumacher, M.A., Pearson, R.F., Møller, T., Valentin-Hansen, P., and Brennan, R.G. (2002). Structures of the pleiotropic translational regulator Hfq and an Hfq-RNA complex: a bacterial Sm-like protein. EMBO J. *21*, 3546–3556.

Seitz, H. (2009). Redefining microRNA targets. Curr. Biol. *19*, 870–873.

Selbach, M., Schwanhäusser, B., Thierfelder, N., Fang, Z., Khanin, R., and Rajewsky, N. (2008). Widespread changes in protein synthesis induced by microRNAs. Nature *455*, 58–63.

Sharma, C.M., Darfeuille, F., Plantinga, T.H., and Vogel, J. (2007). A small RNA regulates multiple ABC transporter mRNAs by targeting C/A-rich elements inside and upstream of ribosome-binding sites. Genes Dev. *21*, 2804–2817.

Shimoni, Y., Friedlander, G., Hetzroni, G., Niv, G., Altuvia, S., Biham, O., and Margalit, H. (2007). Regulation of gene expression by small non-coding RNAs: a quantitative view. Mol. Syst. Biol. *3*, 138.

Shishkin, A.A., Giannoukos, G., Kucukural, A., Ciulla, D., Busby, M., Surka, C., Chen, J., Bhattacharyya, R.P., Rudy, R.F., Patel, M.M., et al. (2015). Simultaneous generation of many RNA-seq libraries in a single reaction. Nat. Methods *12*, 323–325.

Smirnov, A., Wang, C., Drewry, L.L., and Vogel, J. (2017). Molecular mechanism of mRNA repression in *trans* by a ProQ-dependent small RNA. EMBO J. *36*, 1029–1045.

Stern-Ginossar, N., Elefant, N., Zimmermann, A., Wolf, D.G., Saleh, N., Biton, M., Horwitz, E., Prokocimer, Z., Prichard, M., Hahn, G., et al. (2007). Host immune system gene targeting by a viral miRNA. Science *317*, 376–381.

Tree, J.J., Granneman, S., McAteer, S.P., Tollervey, D., and Gally, D.L. (2014). Identification of bacteriophage-encoded anti-sRNAs in pathogenic *Escherichia coli*. Mol. Cell *55*, 199–213.

Updegrove, T.B., Zhang, A., and Storz, G. (2016). Hfq: the flexible RNA matchmaker. Curr. Opin. Microbiol. *30*, 133–138.

Urban, J.H., and Vogel, J. (2007). Translational control and target recognition by *Escherichia coli* small RNAs *in vivo*. Nucleic Acids Res. *35*, 1018–1037.

Urban, J.H., and Vogel, J. (2009). A green fluorescent protein (GFP)-based plasmid system to study post-transcriptional control of gene expression *in vivo*. Methods Mol. Biol. *540*, 301–319.

Vogel, J., and Luisi, B.F. (2011). Hfq and its constellation of RNA. Nat. Rev. Microbiol. *9*, 578–589.

Wagner, E.G. (2013). Cycling of RNAs on Hfq. RNA Biol. *10*, 619–626.

Wagner, E.G.H., and Romby, P. (2015). Small RNAs in bacteria and archaea: who they are, what they do, and how they do it. Adv. Genet. *90*, 133–208.

Wang, J., Rennie, W., Liu, C., Carmack, C.S., Prévost, K., Caron, M.P., Massé, E., Ding, Y., and Wade, J.T. (2015). Identification of bacterial sRNA regulatory targets using ribosome profiling. Nucleic Acids Res. *43*, 10308–10320.

Wright, P.R., Georg, J., Mann, M., Sorescu, D.A., Richter, A.S., Lott, S., Kleinkauf, R., Hess, W.R., and Backofen, R. (2014). CopraRNA and IntaRNA: predicting small RNA targets, networks and interaction domains. Nucleic Acids Res. *42*, W119–W123.

Wroblewska, Z., and Olejniczak, M. (2016). Hfq assists small RNAs in binding to the coding sequence of ompD mRNA and in rearranging its structure. RNA *22*, 979–994.

Zhang, A., Schu, D.J., Tjaden, B.C., Storz, G., and Gottesman, S. (2013). Mutations in interaction surfaces differentially impact *E. coli* Hfq association with small RNAs and their mRNA targets. J. Mol. Biol. *425*, 3678–3697.

STAR★METHODS

KEY RESOURCES TABLE

REAGENT or RESOURCE	SOURCE	IDENTIFIER
Bacterial and Virus Strains		
Escherichia coli K-12 MG1655	General lab strain	MG1655
Escherichia coli K-12 MG1655 $_{laclq}$	Received from S. Altuvia laboratory	MG1655 $_{laclq}$
Escherichia coli K-12 W3110Z1	Expressys	N/A
Escherichia coli K-12 MG1655Z1	Current work	N/A
Escherichia coli K-12 MG1655Z1 *cyaR::Cm*	Current work	Δ*cyaR*
Escherichia coli K-12 MG1655Z1 *gcvB::Cm*	Current work	Δ*gcvB*
Escherichia coli K-12 MG1655Z1 *arcZ::Cm*	Current work	Δ*arcZ*
Escherichia coli K-12 MG1655Z1 *arcZ::Cm*; *hfq-Flag:cat*	Current work	Δ*arcZ hfq-flag*
Escherichia coli K-12 MG1655 *ryhB::Cm*	Current work	MG1655 Δ*ryhB*
Escherichia coli K-12 BW25113	The Keio collection, Baba et al., 2006	BW25113
Escherichia coli K-12 BW25113 *lpp::Kn*	The Keio collection, Baba et al., 2006	BW25113 Δ*lpp*
Escherichia coli K-12 TOP10	Invitrogen	TOP10
Escherichia coli K-12 MG1655Z1 *raiA::Cm*	Current work	Δ*raiA*
Chemicals, Peptides, and Recombinant Proteins		
0.1 mm Glass Beads	BioSpec	Cat #:110079101
Anti-Flag M2 Monoclonal Antibody	Sigma	Cat #: F1804; RRID:AB_262044
RNase A/T1 mix	ThermoFischer Scientific	Cat #: EN0551
T4 Polynucleotide Kinase	New England Biolabs	Cat #: M0236L
T4 RNA ligase 1, High Concentration	New England Biolabs	Cat #: M0437M
RNAClean XP	Beckman Coulter	Cat #: A63987
AMPure XP	Beckman Coulter	Cat #: A63881
Recombinant RNase inhibitor	Takara	Cat #: 2313A
TURBO DNase	ThermoFischer Scientific	Cat #: AM2238
FastAP	ThermoFischer Scientific	Cat #: EF0654
RLT buffer	QIAGEN	Cat #: 79216
Glycoblue	ThermoFischer Scientific	Cat #: AM9516
TriReagent	Sigma-Aldrich	Cat #: T9424
Ultra-pure water, RNase- and DNase-free	Biological Industries	Cat #: 01-866-1A
Acrylamide/Bis-Acrylamide 19:1 40%	Bio-Lab	Cat #: 000135233500
37% Formaldehyde	J.T. Baker	Cat #: 7040.1000
RiboRuler High Range RNA ladder	ThermoFischer Scientific	Cat #: SM1821
pUC18/MspI Marker	ThermoFischer Scientific	Cat #: SM0221
Zeta-Probe Blotting Membranes	Bio-Rad	Cat #: 162-0159
Mini Protean TGX 4-20% gels	Bio-Rad	Cat #: 4568095
Trans-Blot Turbo Transfer Pack	Bio-Rad	Cat #: 1704159
Critical Commercial Assays		
QuikChange Lightning Site-Directed Mutagenesis Kit	Agilent	Cat #: 210519
RiboZero kit for bacteria	Illumina	Cat #: MRZGN126
SuperScript III first strand kit	Invitrogen	Cat #: 18080-051
HIFI HotStart RM	Kapa Biosystems	Cat #: KK2601
Qubit dsDNA HS Assay kit	Invitrogen	Cat #: Q32854
High sensitivity D1000 ScreenTape	Agilent Technologies	Cat #: 5067-5584

(*Continued on next page*)

Continued

REAGENT or RESOURCE	SOURCE	IDENTIFIER
High sensitivity D1000 reagents	Agilent Technologies	Cat #: 5067-5585
Bioanalyzer RNA 6000 Nano kit	Agilent Technologies	Cat #: 5067-1511
Bioanalyzer RNA 6000 Pico kit	Agilent Technologies	Cat #: 5067-1513
RNA clean and Concentrator^{TM}-5 kit	Zymo Research	Cat #: R1016
Deposited Data		
ArcZ comparative RIL-seq	Current work	E-MTAB-8224
Total expression libraries of GcvB, MicA, ArcZ WT, ArcZ M1, ArcZ M2, RyhB and CyaR overexpression	Current work	E-MTAB-8229
Oligonucleotides		
Strain construction oligos	Table S6	N/A
Plasmid construction and mutagenesis oligos	Table S6	N/A
Library preparation oligos	Table S6	N/A
Northern blots probes	Table S6	N/A
Recombinant DNA		
pZE12-luc; Amp^R ; $P_{LlacO-1}$	Expressys	N/A
pMicA; Amp^R ; $P_{LlacO-1}$	Coornaert et al., 2010	N/A
pBRplac; Amp^R ; $P_{LlacO-1}$	Coornaert et al., 2010	N/A
pEF21; Cm^R; P_{BAD}	Received from S. Altuvia lab	N/A
pEF21-Hfq; Cm^R; P_{BAD}	Current work	N/A
pZE12-ArcZ; Amp^R ; $P_{LlacO-1}$	Current work	N/A
pZE12-ArcZ M1; Amp^R ; $P_{LlacO-1}$	Current work	N/A
pZE12-ArcZ M2; Amp^R ; $P_{LlacO-1}$	Current work	N/A
pZE12-CyaR; Amp^R ; $P_{LlacO-1}$	Current work	N/A
pJV300; Amp^R ; $P_{LlacO-1}$	Urban and Vogel, 2007	N/A
pTP-011; Amp^R ; $P_{LlacO-1}$	Urban and Vogel, 2007	N/A
pZA12-GcvB (pJU-014) ; Amp^R ; $P_{LlacO-1}$	Urban and Vogel, 2007	N/A
pXG10-SF; Cm^R; $P_{LtetO-1}$	Corcoran et al., 2012	N/A
pXG-0; Cm^R; $P_{LtetO-1}$	Urban and Vogel, 2007	N/A
pXG10-SF-raiA; Cm^R; $P_{LtetO-1}$	Current work	N/A
pZE12-RaiZ; Amp^R ; $P_{LlacO-1}$	Current work	N/A
pZE12-*raiA*; Amp^R ; $P_{LlacO-1}$	Current work	N/A
pXG10-SF-gatY; Cm^R; $P_{LtetO-1}$	Current work	N/A
pXG10-SF-lpp; Cm^R; $P_{LtetO-1}$	Current work	N/A
Software and Algorithms		
DESeq2	Love et al., 2014	https://bioconductor.org/packages/release/bioc/html/DESeq2.html
RNAup	ViennaRNA package, the University of Vienna	http://rna.tbi.univie.ac.at/cgi-bin/RNAWebSuite/RNAup.cgi
RNAduplex	ViennaRNA package, the University of Vienna	https://www.tbi.univie.ac.at/RNA/RNAduplex.1.html
MEME	Bailey et al., 2009	http://meme-suite.org/tools/meme
R	The R foundation	http://www.r-project.org/
R/ppcor package	Kim, 2015	https://rdrr.io/cran/ppcor/man/pcor.html
Python	The Python Software Foundation	https://www.python.org/
Python/Biopython	Cock et al., 2009	https://biopython.org/

(*Continued on next page*)

Continued

REAGENT or RESOURCE	SOURCE	IDENTIFIER
Blastn	National Center for Biotechnology Information	https://blast.ncbi.nlm.nih.gov/Blast.cgi?PAGE_TYPE=BlastSearch
MUSCLE	Edgar, 2004	https://www.ebi.ac.uk/Tools/msa/muscle/
Conservation profiler script	Current work	https://github.com/YairGatt/ConservationProfiler
RNAfold	ViennaRNA package, the University of Vienna	http://rna.tbi.univie.ac.at/cgi-bin/RNAWebSuite/RNAfold.cgi
Python RILseq package	Melamed et al., 2018	https://github.com/asafpr/RILseq

LEAD CONTACT AND MATERIALS AVAILABILITY

Further information and requests for resources and reagents should be directed to and will be fulfilled by the Lead Contact, Hanah Margalit (hanahm@ekmd.huji.ac.il).

All unique/stable reagents generated in this study are available from the Lead Contact without restriction.

EXPERIMENTAL MODEL AND SUBJECT DETAILS

Bacterial strains used in this work are detailed in the Key Resources Table. Strains were routinely grown with shaking (200 rpm) in LB medium at 37°C. Where appropriate, ampicillin (100 μg/ml), kanamycin (40 μg/ml), chloramphenicol (25 μg/ml) or spectinomycin (50 μg/ml) were added to the growth medium. Bacteria were grown from a single colony overnight, diluted 100-fold in fresh LB medium, and re-grown with shaking (200 rpm) at 37°C to the desired growth phase or condition.

For the construction of the MG1655Z1 strain that carries at its *attB* locus two copies of Lac Repressor and Tet Repressor encoding genes, we used P1 transduction using the *E. coli* K-12 MG1655 as the acceptor strain and the *E. coli* K-12 W3110Z1 (Expressys) as the donor strain. Strains of MG1655Z1 in which sRNA genes are deleted were constructed by the One Step Inactivation method of Datsenko and Wanner (2000), using oligonucleotides 474/475, 472/473, 996/997, 234/235 and 457/458 for *arcZ*, *cyaR, ryhB, gcvB and raiA* deletions, respectively.

METHOD DETAILS

Plasmid construction

The sRNAs and *raiA* sequences were cloned under the $P_{LlacO-1}$ promoter of the pZE12 plasmid, according to Urban and Vogel (2007), enabling induction by IPTG. The pZE12-luc plasmid was PCR amplified using oligonucleotides 167/168 and the PCR product was cleaved by XbaI. A cleavage product containing the origin of replication, the *bla* resistance gene and the $P_{LlacO-1}$ promoter was isolated from an agarose gel and used as a backbone to which sRNA encoding fragments were ligated (Urban and Vogel, 2007). For each sRNA, the sequence starting at the +1 and ending downstream to the terminator was PCR amplified using 5′ phosphate modified oligonucleotide as the forward primer and a XbaI site at the 5′ of the reverse primer. The PCR products were digested using XbaI and ligated to the pZE12 backbone. The oligonucleotides used for sRNA gene amplification were 303/304 (*arcZ*), 308/309 (*cyaR*), 455/456 (*raiZ*) and 454/456 (*raiA*).

Construction of target-*gfp* translational fusions was done as described in Urban and Vogel (2009), using the pXG10-SF as a backbone (Corcoran et al., 2012). For each target gene, a region starting at the main transcription start site (TSS) and encompassing the sites included in RIL-seq chimeras were amplified by PCR, digested with Mph1103I and NheI restriction enzymes and cloned upstream of *gfp* in pXG10-SF digested with the same restriction enzymes. The oligonucleotides used for PCR amplification were 832/833 (*raiA*), 274/1002 (*lpp*) and 731/732 (*gatY*).

Mutagenesis of pZE12-ArcZ was done by the QuikChange Lightning Site-Directed Mutagenesis Kit (Stratagene), using oligonucleotides 482/483 and 575/576 to create pZE12-ArcZ M1 and pZE12-ArcZ M2, respectively.

To construct pEF21-Hfq, *hfq* coding sequence was amplified using oligonucleotides 98/99, the PCR product was digested by PstI and HindIII restriction enzymes and cloned into pEF21 plasmid.

Bacterial strains used in RNA-seq experiments

Generally, the gene expression levels of two types of strains were compared: (1) a strain in which the sRNA is induced for a short time, either from an inducible plasmid (in the studies of GcvB, MicA, ArcZ and CyaR) or from the endogenous chromosomal locus (in the study of RyhB). (2) A control strain in which the sRNA is not induced: a wild-type strain carrying a control plasmid (used in MicA study), or a deletion strain of the sRNA gene carrying a control plasmid (used in GcvB, ArcZ and CyaR studies), or, in the study of RyhB, a

ryhB deletion strain. Strains (1) and (2) were induced for 20 minutes by IPTG (in the studies of GcvB, MicA, ArcZ and CyaR) or by the iron chelator 2,2′-dipyridyl (in the study of RyhB).

Specifically, the GcvB, ArcZ and CyaR expressing plasmids or control plasmids were transformed into an *E. coli* MG1655Z1 strain which, by having two copies of the *lacI*^{q} allele, constitutively expresses high levels of the Lac repressor, and in which the relevant sRNA-encoding gene was deleted. The MicA expressing plasmid and its control plasmid were transformed into an *E. coli* MG1655$_{lacIq}$ that constitutively expresses the Lac repressor, in which the endogenous *micA* was present. RyhB was induced from its endogenous locus. The detailed strains used in the study of each sRNA were as follows: in the GcvB experiment, the Δ*gcvB* strain carrying either pZA12-GcvB or pTP-011 plasmids were used. In the MicA experiment, an MG1655$_{lacIq}$ strain carrying the pEF21-*hfq* plasmid and either the pBRplac or the pMicA plasmids were used (Coornaert et al., 2010). In the ArcZ experiment, a Δ*arcZ hfq-flag* strain carrying either pZE12-ArcZ or pJV300 plasmids were used. In the RyhB experiment, MG1655 and MG1655 Δ*ryhB* strains were used. In the CyaR experiment, the Δ*cyaR* strain carrying either the pZE12-CyaR or the pJV300 plasmids were used.

Culture conditions for RNA-seq experiments

Bacteria were grown to exponential growth phase for GcvB (OD_{600} = 0.3) and for RyhB (OD_{600} = 0.5) induction, or to stationary phase for CyaR and ArcZ (OD_{600} = 1.0) and for MicA (grown for 6 h) induction. GcvB, MicA, ArcZ and CyaR were induced by IPTG (1 mM, 20 min). RyhB was induced by the iron chelator 2,2′-Dipyridyl (200 μM, 20 min). Bacteria were harvested by centrifugation at 4°C, 4500*g* and resuspended in 50 μl TE (10 mM Tris-HCl pH 7.5, 1 mM EDTA). Lysosyme was added to 0.9 mg/ml prior to freezing the sample at liquid nitrogen and storing it at −80°C.

RNA extraction

The frozen samples were subjected to two cycles of thawing at 37°C and refreezing in liquid nitrogen. Next, the samples were resuspended thoroughly to homogenization with 1 mL TriReagent (prewarmed to room temperature) and incubated for 5 min at room temperature. Two hundred microliters of chloroform were added and the tubes content was mixed by inversing the tubes for 15 s. The samples were incubated for 10 min at room temperature, centrifuged (17,000*g,* 10 min at 4°C) and the upper phase was collected and transferred into new Eppendorf tubes. For RNA precipitation, 500 μl isopropanol was added, the tube contents were mixed thoroughly by inversion of the tubes and incubated for 10 min at room temperature. The tubes were centrifuged (17,000*g*,15 min at 4°C) and the supernatant was discarded. The pellets were washed twice by addition of 1 mL of freshly made 75% (vol/vol) ethanol, followed by centrifugation (17,000*g* for 5 min at 4°C) and removal of the supernatant. Pellets were dried by leaving the tubes open for 15 min at room temperature, and then re-suspended in 300 μL nuclease free water and stored at −20°C. The RNA concentration was measured using Nanodrop (ThermoFisher Scientific).

RNA sequencing

Library construction and sequencing

The experiments were performed in triplicates for each strain. RNA-seq libraries were constructed according to the RNAtag-Seq protocol (Shishkin et al., 2015) with several modifications to enable capturing of short RNA fragments (Melamed et al., 2018). The library molar concentration was calculated according to the weight/volume concentration and the average cDNA fragment size, measured by Qubit™ dsDNA HS Assay Kit (Invitrogen) and TapeStation High Sensitivity D1000 ScreenTape (Agilent) analyses, respectively. 1300 μl of 1.8 pM denatured library was loaded on Nextseq500 Sequencer (Illumina). The libraries of GcvB, ArcZ, RyhB and CyaR induction and corresponding control libraries were sequenced by single-end sequencing of 85 bases, while the libraries of MicA induction and control libraries were sequenced by paired-end sequencing of 45 bases of Read 1 and 40 bases of Read 2.

Sequencing data analysis

Raw reads were split into their library of origin using the barcode sequences at the beginning of the read (first read in case of paired-end sequencing). The single or paired reads were then processed by cutadapt (Martin, 2011) to remove low-quality ends and adaptor sequences. The fragments were mapped to the genome of *E. coli* K12 MG1655 (RefSeq accession number NC_000913.3) using bwa aln followed by bwa sampe for paired-end sequencing or samse for single-end sequencing (Li, 2013). A custom script was used to retrieve the count files from the bwa files.

For calculating the total expression, the number of reads mapped to the region that was involved in the chimeric fragment was counted and normalized by its length. In case an interaction was identified in multiple locations along the target, the total expression values were normalized by this number.

ArcZ comparative RIL-seq

The RIL-seq experiment was performed as described in Melamed et al. (2016) and in details in Melamed et al. (2018)*:* Δ*arcZ hfq*-Flag strain was transformed with a ArcZ WT (pZE12-ArcZ), ArcZ C71G (pZE12-ArcZ M1) or a ArcZ C71U,U72G,G73A (pZE12-ArcZ M2) plasmids. Single colonies of the transformants were grown overnight in LB at 37°C with shaking (200 rpm). Cultures were diluted 100-fold in fresh LB, re-grown with shaking at 37°C to stationary phase (OD_{600} = 1.0) and induced with IPTG (1mM, 20 min). Total expression libraries of the same cultures, including control samples of the Δ*arcZ hfq*-Flag strain with pJV300 plasmid, were performed as described above, each repeated three times.

The comparative RIL-seq libraries were sequenced by paired-end sequencing of 45 bases for Read 1 and 40 bases for Read 2 and the total expression libraries were sequenced by single-end sequencing of 85 bases, using Nextseq500 Sequencer (Illumina).

The sequenced reads were mapped to the *E. coli* K-12 MG1655 chromosome (RefSeq accession number NC_000913.3) and to the relevant plasmid sequence. A unified library of the three replicates of each strain was used for the analyses in Figure 3.

Northern analysis

For the study of *raiA*, a Δ*raiA* strain carrying either pZE12-raiA, pZE12-RaiZ or pJV300 plasmids were used. For the study of *lpp*, BW25113 and BW25113 Δ*lpp* strains were used (Baba et al., 2006). RNA samples (20 μg) were heated for 10 min at 65°C in loading buffer (final concentration of 65% formamide), separated on 7 M urea and 6% polyacrylamide gels in 0.5X TBE buffer (45 mM Tris-base, 45 mM Boric acid and 2 mM EDTA pH 8.0), and electro-transferred to a Zeta-Probe membrane (Bio-Rad). The membranes were hybridized with specific [^{32}P] end labeled DNA oligonucleotides in Church buffer (500 mM sodium phosphate buffer pH 6.5, 7% SDS, 10 mg/ml Bovine serum albumin) at 45°C, washed twice with 3X SSC (45 mM Na-citrate, 45 mM NaCl, pH 7.0) and visualized by GE Typhoon Phosphorimager. The sequences of the oligonucleotides are listed in Table S6. For *lpp*, two probes were used in the same hybridization (986 and 987).

GFP reporter assay

The GFP reporter assays were done essentially as described previously (Corcoran et al., 2012; Urban and Vogel, 2009). Wild-type TOP10 (Invitrogen) cells were transformed with two plasmid types: (1) a low copy number plasmid expressing the target-GFP (pXG10 plasmids), and (2) a high copy number plasmid expressing the sRNA (pZE12 for CyaR and RyhB and pZA12 for GcvB). Control plasmids were a non-GFP plasmid (pXG0) and sRNA control plasmid (pTP011 for GcvB and pJV300 for all other studied sRNAs). See Key Resources Table. Single colonies were grown overnight, diluted 1:100 in fresh medium and grown at 30°C to OD_{600} = 0.5. One ml of each culture was centrifuged and the pellet was resuspended in 300 μl of 1X PBS. Fluorescence was measured using the BD AccuriTM flow cytometer. Change in fluorescence level in response to the sRNA was expressed as the ratio of the fluorescence level of cells that overexpress the sRNA and cells that carry the control plasmid (after subtraction of the auto-fluorescence). For every sRNA-target combination, experiments were done for three biological repeats.

QUANTIFICATION AND STATISTICAL ANALYSIS

Differential expression analysis using DESeq2

To compare gene expression levels before and after overexpression of the sRNA, differential expression analysis was performed using the DESeq2 package in R (Love et al., 2014). Based on the differential expression analysis, the targets were divided into two subsets: targets that showed a statistically significant change in their expression levels and targets that were statistically significantly unchanged in their expression levels. To determine the first subset, we used the results function with the default values, considering padj < 0.1 as a significant change. To determine the second subset of genes we used the results function with the parameter lfcThreshold = 0.5 for MicA and GcvB or lfcThreshold = 1 for ArcZ, RyhB and CyaR along with the parameter altHypothesis = lessAbs. Genes that could not be assigned unambiguously to one of these two subsets were excluded from the analysis.

Wilcoxon rank sum test, Hypergeometric test, Spearman correlation and Spearman partial correlation

Wilcoxon rank sum test, Hypergeometric test and Spearman correlation were carried out by R using wilcox.test, phyper, cor.test functions, respectively (R Core Team, 2017). The Wilcoxon rank sum test was one sided. The partial correlation was calculated using the pcor.test function from the ppcor R package (Kim, 2015).

Identification of a common motif in the target sets

The sequences of RIL-seq targets of ArcZ WT, ArcZ M1 and ArcZ M2 were subjected to a search for a common motif by MEME (Bailey et al., 2009). The best MEME motif for every strain is shown in Figure 3.

Prediction of RNA secondary structure

The secondary structures of ArcZ WT, of ArcZ M1 and of ArcZ M2 were predicted using RNAfold (Lorenz et al., 2011) and are shown in Figure S2A.

Sequence conservation analysis of binding sites

In order to assess the evolutionary conservation of the binding sites of the affected and unaffected targets we constructed a multiple sequence alignment (MSA) for each binding site and computed its respective information content. We first extracted reference sequences from the genome of *E. coli* K12 MG1655 (NC_000913.2) for all sRNAs and targets of interest and identified the binding site motif for each target using MAST. Blastn (Camacho et al., 2009) was then used twice: 1. to query each reference sequence against a database of 1118 complete Enterobacteriaceae genomes from NCBI's RefSeq database (O'Leary et al., 2016) and compile the top hits for each genome, adhering to stringent thresholds of e-value < 0.01, identity percentage > 0.4, and aligned length > 50% of the query sequence. 2. To query each binding site against the first blastn results for that target and identify the corresponding binding site regions in each strain. Finally, we aligned the identified regions using MUSCLE (default parameters) (Edgar, 2004) to construct a multiple sequence alignment. Upstream and downstream sequences identical in length to the binding site were similarly blasted against

all strains and aligned as a control. We assessed the degree of conservation of each region from the MSA by Information Content computation (Schneider and Stephens, 1990; Schneider et al., 1986). Information content was calculated for each position using functions from the Biopython toolkit (Cock et al., 2009) according to the following formula:

$$IC_j = \sum_{i=1}^{N_a} P_{ij} \log\left(\frac{P_{ij}}{Q_i}\right)$$

Where IC_j is the information content for the j^{th} position in an alignment, N_a is the number of letters in the alphabet, P_{ij} is the frequency of a particular letter i in the j^{th} position. Q_i is the expected frequency of a letter i (here Qi was set to 0.25, which applies to *E. coli* and the other bacteria in the alignments). The information content of each region was calculated as the average of the information content values of the positions within the region. The information content of the different regions was also normalized by two measures derived from the results of the two blastn runs: 1. The number of hits for the target in the first run out of all the strains in the database. 2. The number of hits for the region in the second run out of all the hits for the target in the first run. There were very slight differences between the results by the two normalizations.

Binding free energy computation

Binding free energy value (kcal/mol) between two interacting RNAs was computed by RNAup (Mückstein et al., 2006) and by RNAduplex (Lorenz et al., 2011). For RNAup calculation, the sRNA and target sequences were extracted based on the genome coordinates of the chimeric fragments, as reported in Table S2 in Melamed et al. (2016). Computation was done with padding of 20 nucleotides at the ends of chimeras. For RNAduplex calculation, the free energy was calculated between the binding site of the sRNA as reported in Table S4 in Melamed et al. (2016) and the binding site of the target (Table S4). Coordinates were based on the genome of *E. coli* K12 MG1655 (NC_000913.2).

DATA AND CODE AVAILABILITY

The sequencing data of the ArcZ comparative RIL-seq and of all total RNA expression libraries generated in this study are available at ArrayExpress. The accession number for the RIL-seq data is ArrayExpress: E-MTAB-8224. The accession number for the total RNA expression data is ArrayExpress: E-MTAB-8229.

The Conservation profiler script used for sequence conservation analysis of binding sites is available at GitHub, https://github.com/YairGatt/ConservationProfiler.

Cell Reports, Volume *30*

Supplemental Information

Hierarchy in Hfq Chaperon Occupancy of Small RNA Targets Plays a Major Role in Their Regulation

Raya Faigenbaum-Romm, Avichai Reich, Yair E. Gatt, Meshi Barsheshet, Liron Argaman, and Hanah Margalit

TABLE OF CONTENTS

Figure S1. Some RyhB targets are unaffected both at the mRNA and the translational level

Figure S2. Analysis of ArcZ mutants

Figure S3. sRNA binding sites of affected and unaffected targets show similar evolutionary conservation degrees

Figure S4. Detailed experiments exploring steady interactions that do not lead to changes in the target RNA level

Supplementary Figures

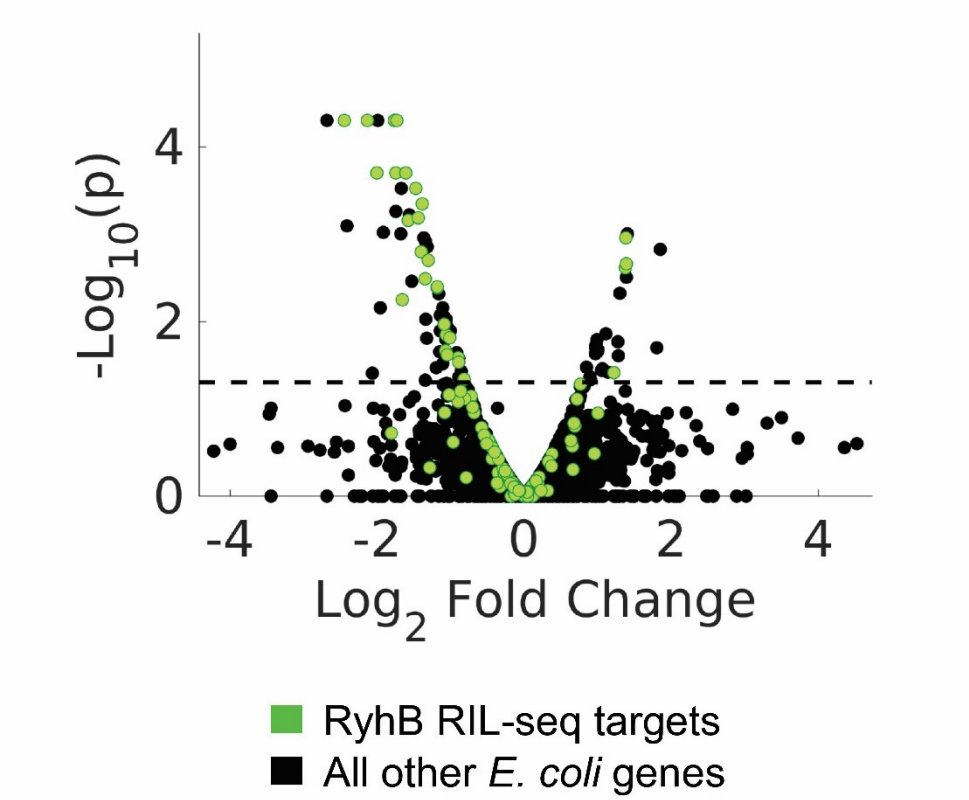

Figure S1 (related to Figure 2). Some RyhB targets are unaffected both at the mRNA and the translational level. Shown is a Volcano plot of ribosome-profiling results of translational level change following RyhB overexpression, based on ribosomal-profiling data of Wang et al. (2015). The translational level change of each gene is represented by the Log_2 Fold Change (Wang et al., 2015). The statistical significance of the change is represented as $-\log_{10}p$ (y axis). Green dots represent the RyhB targets detected by RIL-seq applied to *E. coli* grown to exponential phase under iron limitation. Black dots represent the rest of *E. coli* genes. The dashed line represents the statistical significance threshold set by Wang et al. (2015) ($p \leq 0.05$).

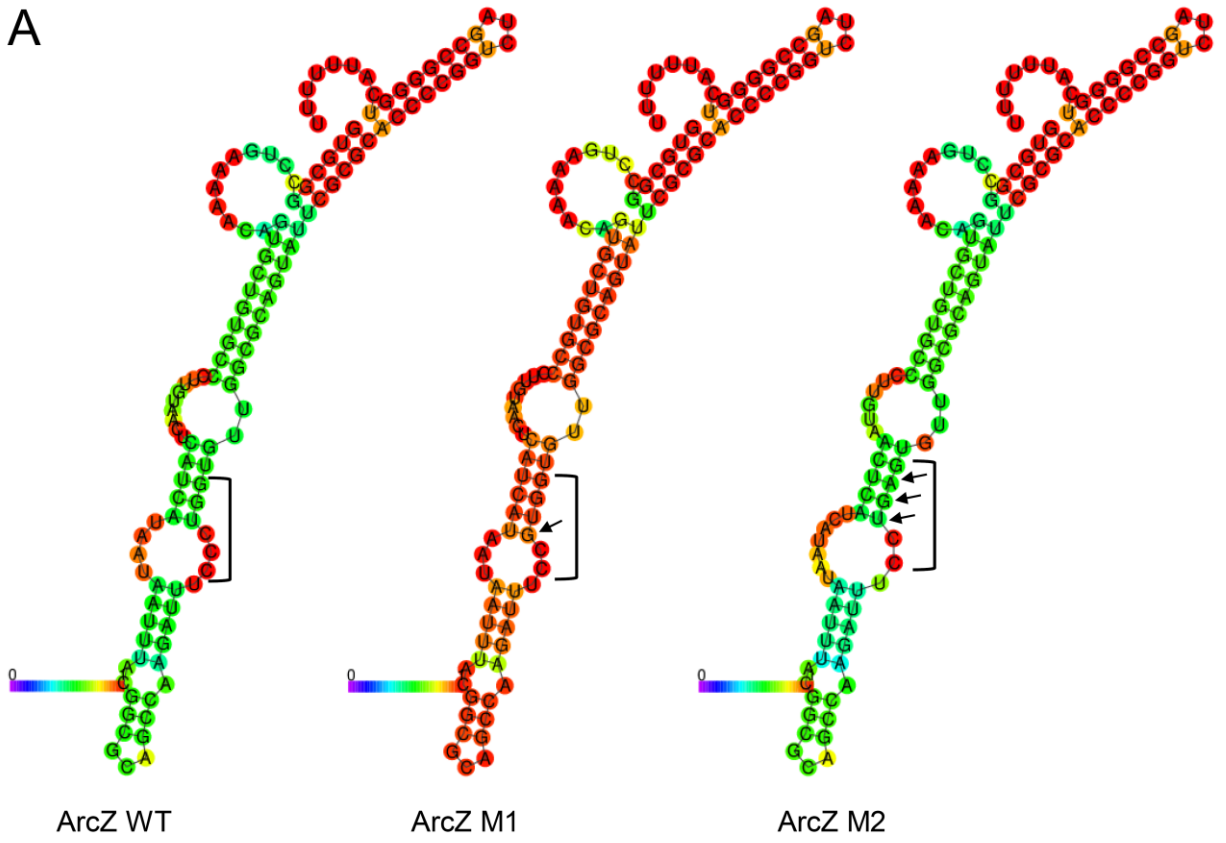
A
ArcZ WT
ArcZ M1
ArcZ M2

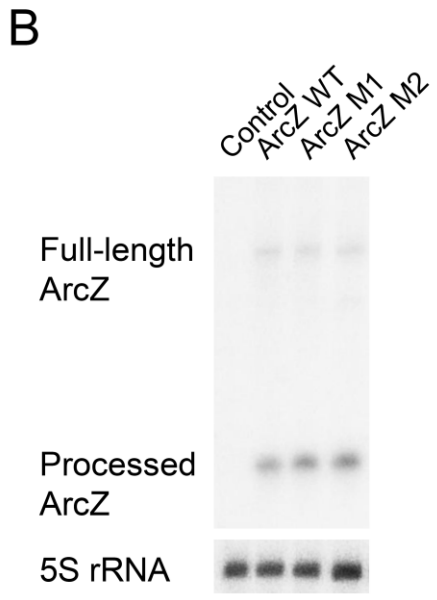
B
Control
ArcZ WT
ArcZ M1
ArcZ M2
Full-length ArcZ
Processed ArcZ
5S rRNA

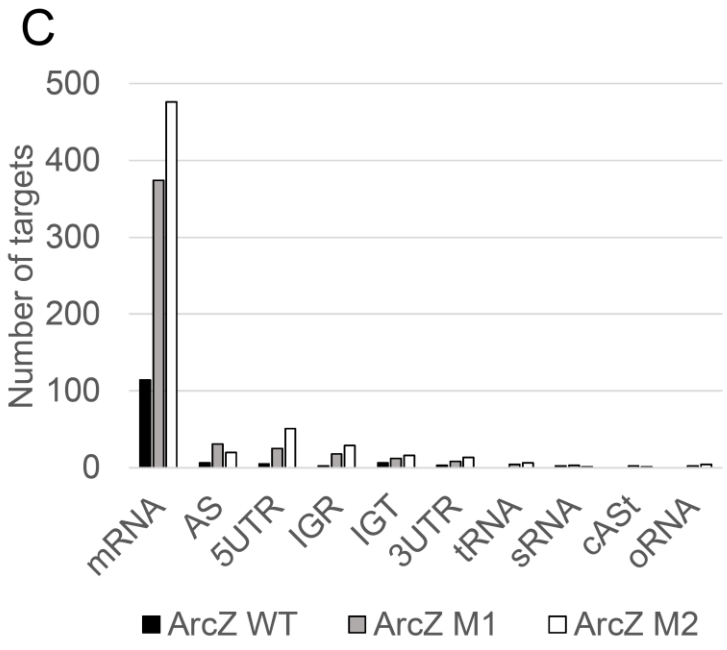
C
Number of targets
500
400
300
200
100
0
mRNA
AS
5UTR
IGR
IGT
3UTR
tRNA
sRNA
cASt
oRNA
ArcZ WT
ArcZ M1
ArcZ M2

Figure S2 (related to Figure 3). Analysis of ArcZ mutants. (A) The predicted secondary structures of ArcZ wild type and mutants are similar. The secondary structures of ArcZ WT, ArcZ M1 and ArcZ M2 were predicted using RNAfold (Lorenz et al., 2011). Colors represent computed base pairing probabilities, with red color for the highest probability. The binding site is marked with a bracket; the mutations are marked with arrows. (B) The cellular levels of ArcZ WT, ArcZ M1 and ArcZ M2 are similar, as shown by northern blot analysis using total RNA extracted from a Δ*arcZ* strain carrying pJV300 (Control), pZE12-ArcZ WT, pZE12-ArcZ M1 or pZE12-ArcZ M2 plasmids grown to OD_{600}=1.0 and induced with IPTG for 20 min. 5S rRNA was probed as a loading control. (C) Classification of RIL-seq targets of ArcZ WT, ArcZ M1 and ArcZ M2 into ten major categories: 5UTR (5' untranslated region), CDS (coding sequence), 3UTR (3' untranslated region), tRNA, sRNA, oRNA (other non-coding RNAs), AS (antisense), cASt (cis antisense with putative trans target), IGR (intergenic region), and IGT (intergenic within transcript). Bars represent the number of targets classified to each category.

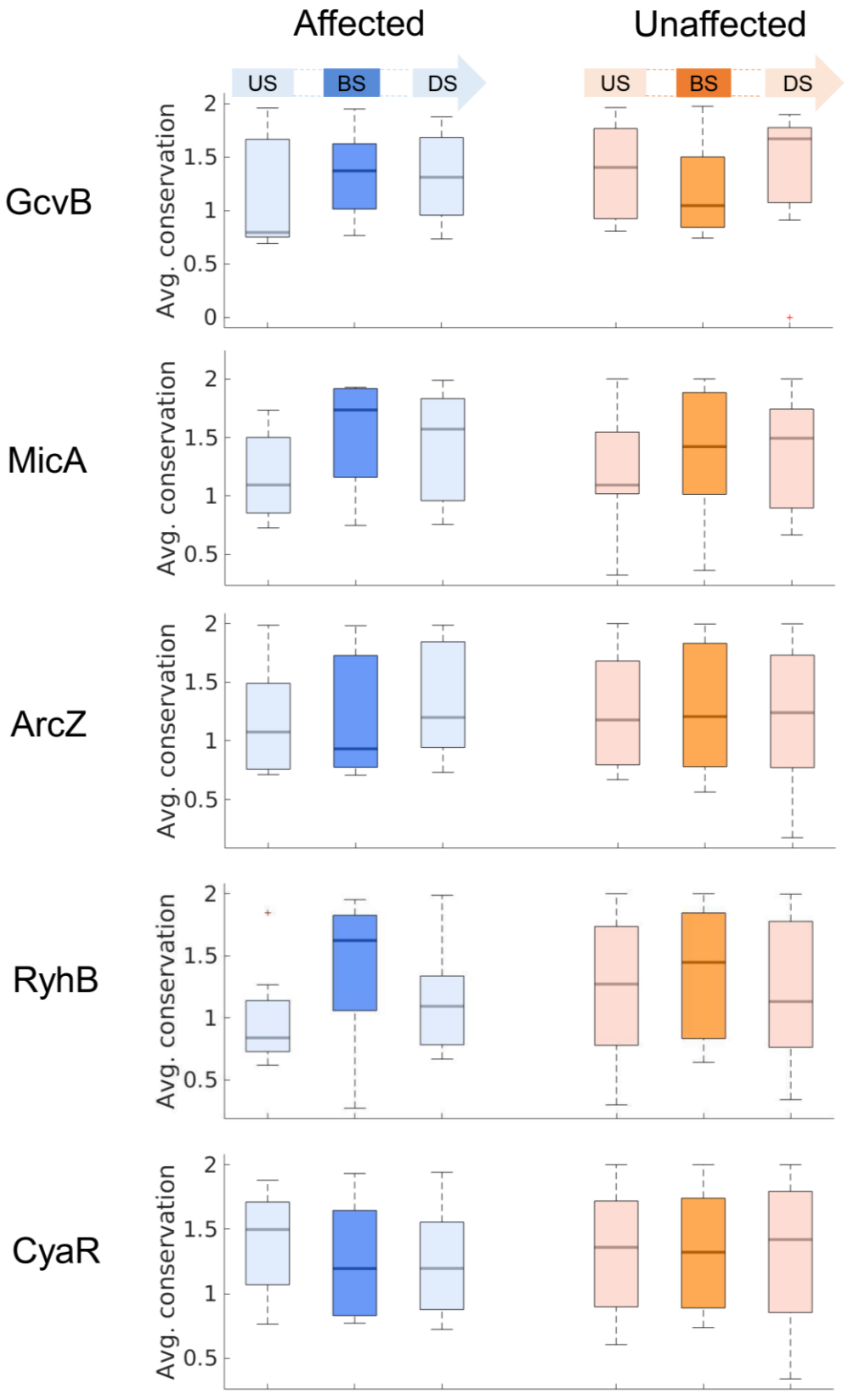
Affected
Unaffected
US
BS
DS
US
BS
DS
GcvB
MicA
ArcZ
RyhB
CyaR
Avg. conservation
0
0.5
1
1.5
2

Figure S3 (related to Figure 2). sRNA binding sites of affected and unaffected targets show similar evolutionary conservation degrees. For all tested sRNAs, the conservation degrees (represented by the average information content) of the affected targets (blue) and the unaffected targets (orange) were high and did not differ statistically significantly between the two subsets. The conservation degrees of their flanking sequences (light blue for affected targets and light orange for unaffected targets) were used as a control. For all sRNAs both flanking regions did not differ statistically significantly in their conservation degrees from the binding sites for both affected and unaffected subsets. Statistical significance was assessed by Wilcoxon rank sum test. US, upstream sequence, BS, binding site, and DS, downstream sequences.

A

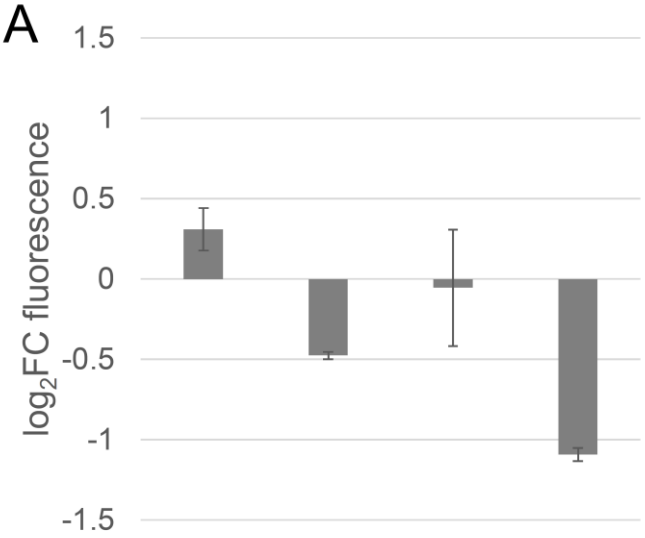

sRNA	CyaR	RyhB	GcvB	GcvB
Fused target	*lpp*	*lpp*	*raiA*	*gatY*

B

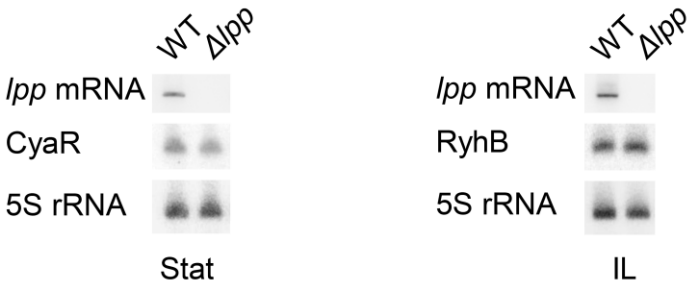

C

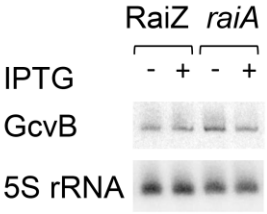

D

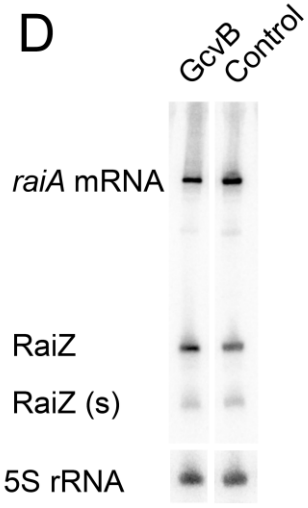

Figure S4 (related to Figures 1 and 2): Detailed experiments exploring steady interactions that do not lead to changes in the target RNA level. (A) Testing the effect of a sRNA on its target protein level using target-*gfp* translational fusion: bacteria carrying a target-*gfp* fusion expressing plasmid and a sRNA overexpressing plasmid or a control plasmid were grown at 30 ºC to exponential phase (OD_{600} = 0.5) and the GFP intensities were measured. The log_2 fold change values (log_2FC) between GFP fluorescence in cells overexpressing the sRNA and cells carrying a control plasmid are presented. Error bars indicate standard deviations based on three independent repeats. (B) *lpp*-mRNA levels do not affect the levels of CyaR and RyhB. BW25113 and BW25113 Δ*lpp* cells were grown to stationary phase (Stat; OD_{600}=1.0) or to exponential phase (OD_{600}=0.5) subjected to iron limitation (IL, 200 μM 2,2'-dipyridyl for 30 min). Total RNA was extracted and 30 μg RNA were analyzed by northern blots, using radiolabeled probes for *lpp*, CyaR, RyhB and 5S rRNA. (C) RaiZ and *raiA*-mRNA levels do not affect the levels of GcvB. Δ*raiA* cells carrying pZE12-RaiZ or pZE12-*raiA* plasmids were grown to exponential phase (OD_{600}=0.5) and induced with IPTG (1mM, 30 min). Total RNA was extracted and analyzed as in (B) using radiolabeled probes for GcvB sRNA and 5S rRNA. (D) GcvB sRNA does not affect RaiZ or *raiA* mRNA. Δ*gcvB* cells carrying pZA12-GcvB or pTP011 (control) plasmids were grown to exponential phase (OD_{600}=0.5) and induced with IPTG for 15 min. Total RNA was extracted and analyzed as in (B) using radiolabeled probes for *raiA*/RaiZ and 5S rRNA (loading control). RaiZ-S is a processing product of RaiZ.